

Searching for a source without gradients: how good is infotaxis and how to beat it

Aurore Loisy* and Christophe Eloy†

Aix Marseille Univ, CNRS, Centrale Marseille, IRPHE, Marseille, France

(Dated: April 15, 2022)

Infotaxis is a popular search algorithm originally designed to track a source of odor in a turbulent environment using information provided by odor detection events gathered along the search. To exemplify its capabilities, the source-tracking task was framed as a partially observable Markov decision process consisting in finding, as fast as possible, a stationary target hidden in a 2D Cartesian grid using stochastic partial observations of the target location. Infotaxis, which states that the searcher should act such as to maximize information about the target location, was shown to be superior to more naive strategies, such as going to the more likely source location. Yet no quantitative assessment of its performance has been reported. Here we provide an extended review of infotaxis, together with a toolkit for devising better strategies. We first generalize the source-tracking task to any number of space dimensions and evaluate thoroughly the performance of infotaxis in domains from 1D to 4D. Our results show that, while being suboptimal, infotaxis is reliable (the probability of not reaching the source approaches zero), efficient (the mean search time scales as expected for the optimal strategy), and safe (the tail of the distribution of search times decays faster than any power law, though subexponentially). We then take on the challenge of beating infotaxis. We present three methods that succeed and evaluate the resulting strategies. First, we formulate the multi-step generalization of infotaxis, and show that its performance is not a monotonic function of the anticipated number of steps. We then propose a more efficient heuristic, called space-aware infotaxis, that beats infotaxis in most cases without any additional parameter. Finally we show how deep reinforcement learning can be used to find optimal (or near optimal) solutions, and compare those solutions to infotaxis. Altogether, our results demonstrate that the margin of improvement toward the optimal strategy gets smaller as the dimensionality increases for reasons which we discuss. Beyond the source-tracking problem, our work illustrates how methods from artificial intelligence can be leveraged to solve decision-making problems constrained by physics, as routinely encountered in biophysics and robotics.

I. INTRODUCTION

Tracking down a source of odor in a turbulent environment is a task performed by many flying and swimming animals [1–4]. In the hope of uncovering the search algorithms used by Nature, Vergassola et al. [5] formulated what we will refer to as the “source-tracking problem”. The modeling of this biology-inspired problem heavily relies on physics. Its solutions, however, call for methods of operations research, automated planning and artificial intelligence. Our first goal here is to make this problem and its solutions accessible to these different communities which are not always aware of each other’s work.

A source that emits a chemical substance, such as an odor, in a quiescent fluid generates a smooth concentration field that decays with the distance to the emission point. This source is easily tracked, because one only needs to follow concentration gradients: this behavior, ubiquitous in biology, is called chemotaxis. Source-tracking becomes much harder in a turbulent medium, because the concentration field consists of disconnected patches of high concentration, randomly distributed and separated by voids. An animal able to detect concentration levels would receive a highly intermittent signal consisting of sharp peaks separated by long periods with

no measurable concentration [6]. Gradient-based strategies are therefore doomed to fail.

To mimic these searching conditions in a computation-friendly environment, Vergassola et al. [5] designed the source-tracking problem. It consists in minimizing the number of steps (cumulated cost) to reach a source (target) hidden in a discrete grid. At each step, the searcher (agent) moves to a neighbor cell (action) and receives a stochastic sensory signal (observation, called “hits”). This signal provides a noisy information about the distance to the source (stochastic partial information). The agent knows how observations are generated (the model), and has a perfect memory of past observations and actions, therefore it can maintain a probability distribution over source locations (belief) updated after each observation using Bayes’ inference theorem. Solving this problem consists in finding the optimal strategy (policy), defined as the mapping from belief to action, that minimizes the expected number of steps to reach the source.

In the language of artificial intelligence and related disciplines, the source-tracking problem is a partially observable Markov decision process (POMDP) which is framed as a belief-MDP (a MDP – Markov decision process – where states are replaced by belief states). It actually belongs to a narrower class of problems, called partially observable stochastic shortest path problems, for which a few formal mathematical results exist, namely: the existence of a deterministic policy that is optimal within the class of Markov policies, and the pointwise

* aurore.loisy@irphe.univ-mrs.fr

† christophe.eloy@centrale-marseille.fr

convergence of value iteration to the unique bounded fixed point of the dynamic programming operator [7, 8].

Yet computing the optimal policy is not feasible: POMDP exact solvers take prohibitively large amounts of computation time for any but the smallest problems [9–12], and the continuous nature of the belief space prevents the use of exact methods for tabular MDPs (e.g. value iteration). Approximate solution methods exist [11–14], but scalability remains an issue. An alternative is deep reinforcement learning: originally designed to solve MDPs using a neural network approximation of the value function [15], existing algorithms can account for partial observability using the belief-MDP formulation.

On the other hand, heuristic policies can be hand-crafted using intuition and knowledge. Infotaxis is a such a heuristic: it states that the agent should choose the action from which it expects the greatest information gain about the source location. The physical intuition behind this algorithm is, quoting the authors, that “information accumulates faster close to the source because cues arrive at a higher rate, hence tracking the maximum rate of information acquisition will guide the searcher to the source much like concentration gradients in chemotaxis” [5].

The infotaxis policy is more precisely defined as the policy that maximizes the expected gain of information, defined as the decrement of Shannon entropy of the belief, over a 1-step horizon. In other words, infotaxis is an information-greedy policy. The idea of information maximization (or, equivalently, uncertainty minimization) using a probabilistic formulation can be traced back to Cassandra et al. [16] who proposed it as a heuristic for robot navigation in uncertain environments, and it has since become a central concept for robotic exploration algorithms [17].

Infotaxis is generally believed to be robust and has become a popular search algorithm. It has been implemented in robots [18, 19] and has inspired various extensions: infotaxis on different types of lattices [20, 21], continuous-space infotaxis [22], mapless infotaxis [19], collective infotaxis [20], socialtaxis [23], entrotaxis [24], infotaxis with an energetic cost [25], and possibly others we have missed. Its relevance to biological searches remains very speculative, but some attempts have been made to explain the trajectories of moths [5, 26] and of the worm *C. elegans* [27] by infotactic searches.

Yet, the (supposedly) good performance of infotaxis is somewhat surprising: there is, a priori, no reason why greedily reducing uncertainty should minimize the time to reach the source (unless the two were linearly related, it is easy to check that they are not). Besides, infotaxis is known not to be optimal and that better performance can be achieved by shifting it toward a more exploitative behavior [19, 20], though no satisfying way (i.e. parameter-free) of doing this has been proposed so far.

It may therefore be even more surprising that the performance of infotaxis has never been evaluated in a sys-

tematic manner. Several papers implemented (variants of) the algorithm [20–22, 24, 28–30], and some tested its robustness to model uncertainty [20, 24, 28, 30], but no performance review exists to date. In addition, most of these prior studies applied infotaxis to searches in 2D domains: very few considered the 3D problem [22, 29], and none tested the algorithm in 1D. The questions of how infotactic trajectories are affected by dimensionality and whether infotaxis generalizes well to high dimensional spaces are still unanswered.

In this paper, our main contributions are the following.

- We generalize the source-tracking problem to any space dimension and provide its complete formulation (which has never been published in details).
- We introduce a protocol for a proper evaluation of infotaxis performance (in particular it is not affected by finite-size effects or by an arbitrarily chosen initial distance to the source) and we propose an efficient method to compute the distribution of arrival times.
- Using this protocol, we compute and analyze the performance of infotaxis as a function of the problem dimensionality (from 1D to 4D) and of the relevant parameters which govern the physics of odor propagation and detection.
- We generalize infotaxis to an N-step (rather than a 1-step) horizon and determine to which extent increasing computational complexity can improve performance on the source-tracking task.
- We build on infotaxis to propose a new parameter-free heuristic policy, “space-aware infotaxis”, which beats infotaxis in most cases.
- We use deep reinforcement learning to determine approximately optimal policies for this task and compare the performance of those learned policies to infotaxis.

As we shall see, the lack of directionality in the information provided by observations makes the source-tracking problem particularly challenging. Our results provide extensive evidence that, while being suboptimal, infotaxis has three important properties: (i) reliability (the probability of never finding the source approaches zero), (ii) efficiency (the mean search time scales as expected for the optimal policy), and (iii) safety (in the sense that arrival times are not plagued by large fluctuations). The performance of space-aware infotaxis and of (near) optimal policies obtained by reinforcement learning strongly suggest that while infotaxis is vastly suboptimal in 1D, the margin of improvement toward the optimal policy gets tighter as the dimensionality increases. The reasons behind this increasingly good performance are discussed in the last section.

Our various (successful) attempts at designing strategies better than infotaxis are based on well-established

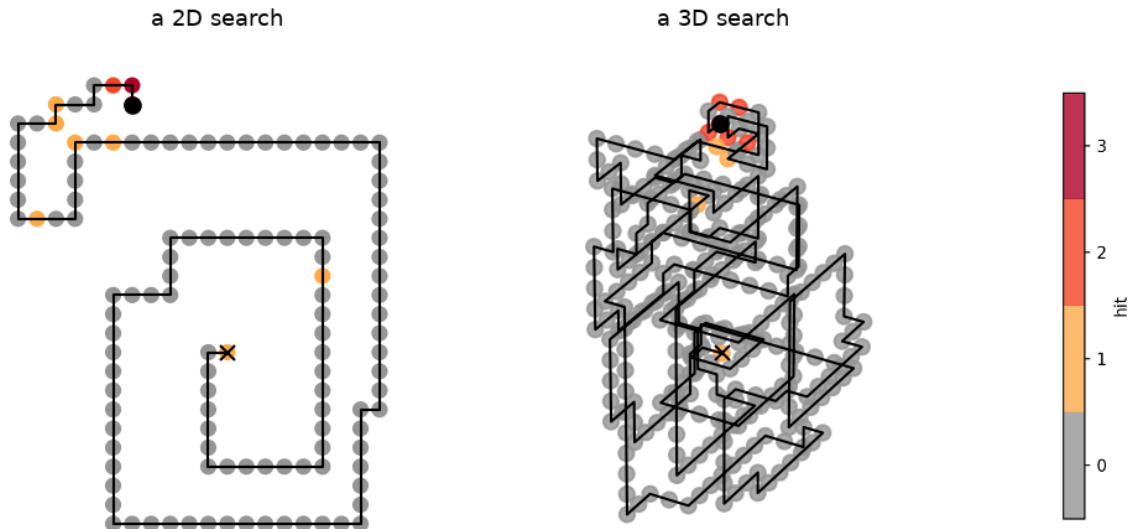


FIG. 1. Examples of trajectories in the source-tracking problem, where a searcher (agent) must find a source (hidden target) using information provided by odor detections called “hits” (partial observations). The start of the search is indicated by a cross, and the end of the search (source location) is depicted by a black dot. These trajectories were generated using the infotaxis policy. Videos are provided in Supplemental Material.

techniques from operations research, automated planning, and artificial intelligence: (i) tree search based on an existing heuristic (N-step infotaxis), (ii) knowledge-based approximation of the optimal value function (space-aware infotaxis), and (iii) deep reinforcement learning. Throughout this paper we explain how to apply these methods to the source-tracking problem. This is, however, only an illustration of their capabilities: the very same approaches can be used for any physics-constrained problem involving decision-making with partial information, such as those faced by animals with sensory organs, or by robots equipped with on-board sensors.

II. THE SOURCE-TRACKING POMDP

A. Overview

The source-tracking problem, illustrated in Fig. 1, is a POMDP in which the agent seeks to identify the true location of an imperfectly observed stationary target (a source of odor). The environment is an n -dimensional Cartesian grid and the source, invisible to the agent, is located in one of the cells. At each step, the agent moves to a neighbor cell and receives an observation, which is a noisy measurement of its distance to the source. The search continues until the agent moves to the cell occupied by the source. The agent has a perfect memory and a perfect knowledge of the process that generates observations. How should the agent behave in order to reach the source in the smallest possible number of steps?

We denote \mathbf{x}^s and \mathbf{x}^a the source and the agent loca-

tions (n -tuples of integers), respectively. Allowed actions are moves to a neighbor cell along the grid axes, for example in 3D the set of allowed actions is {‘north’, ‘south’, ‘east’, ‘west’, ‘top’, ‘bottom’} (staying in the same location is not allowed). After moving to a cell, either the source is found (event F) and the search is over, or the source is not found (complementary event \bar{F}) and the agent receives a stochastic sensor measurement h (“hit”), which represents the integer number of odor particles detected by the agent. Hits are received with conditional probability $\Pr(h|\mathbf{x}^a, \mathbf{x}^s)$ (the probabilistic model of detection will be presented in Section II C). We encompass the presence/absence of the source and the number of hits in a single observation variable o . Possible observations are $o \in \{F, (\bar{F}, 0), (\bar{F}, 1), (\bar{F}, 2), \dots\}$.

We denote $p(\mathbf{x})$ the discrete probability distribution of the source being in each grid cell, that is $p(\mathbf{x}) = \Pr(\mathbf{x} = \mathbf{x}^s)$. After each action and observation, $p(\mathbf{x})$ can be updated using Bayesian inference (see Section II D). The agent has access to its position \mathbf{x}^a and to the distribution $p(\mathbf{x})$. In the POMDP terminology, this defines a belief state $s = [\mathbf{x}^a, p(\mathbf{x})]$. Examples of belief states are shown in Fig. 2. Finding the source results in a special belief state s^Ω where the source’s position is known and matches the agent’s position: $s^\Omega = [\mathbf{x}^a, \delta(\mathbf{x} - \mathbf{x}^a)]$. The agent’s behavior is described by a policy, denoted π , which maps each belief state to an action. For a deterministic policy (as sought here, since the optimal policy is deterministic), the action chosen is $a = \pi(s)$.

The search proceeds as follows:

- Initially
 - The belief state is $s_0 = [\mathbf{x}_0^a, p_0(\mathbf{x})]$, where

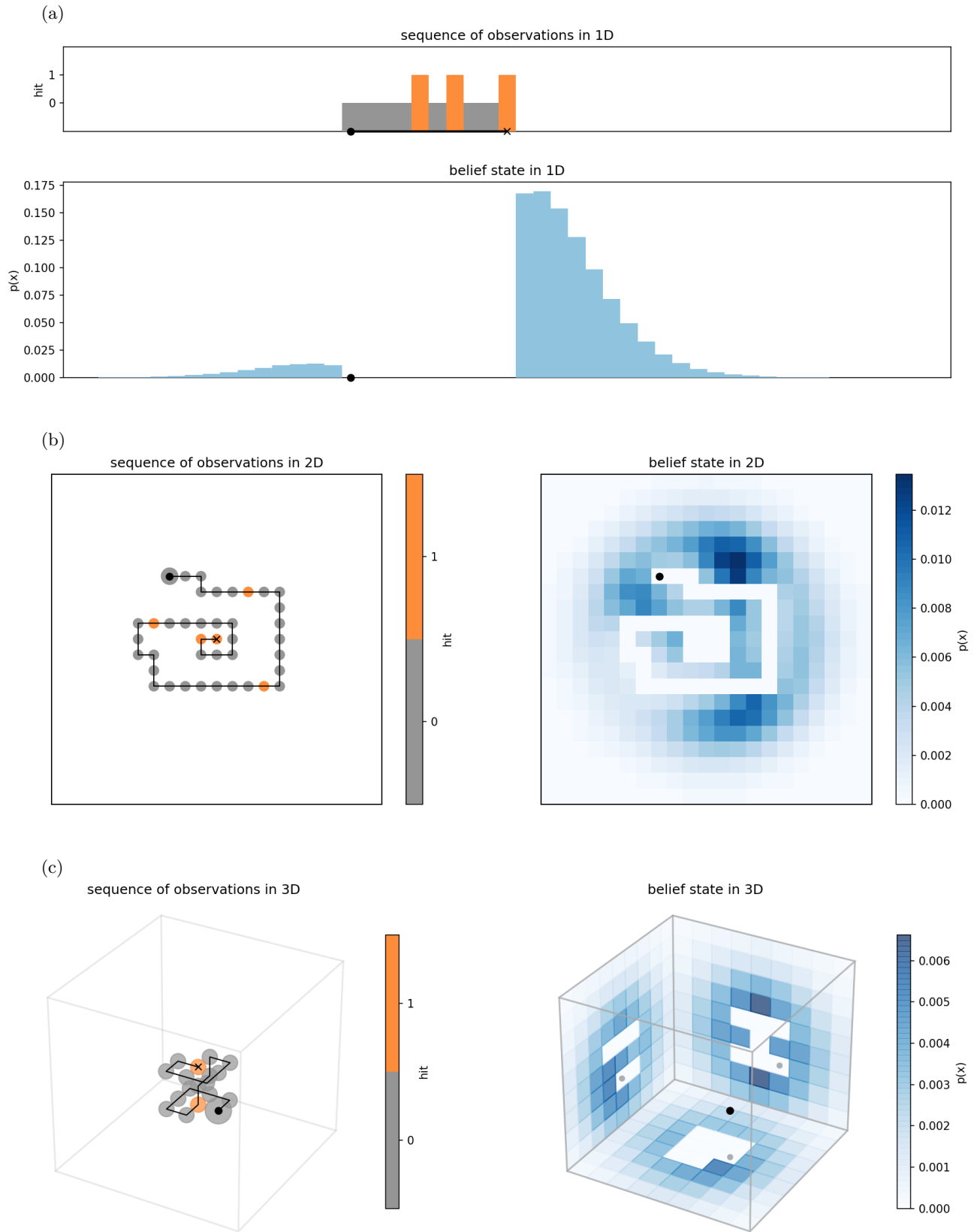


FIG. 2. Examples of observation sequences and of corresponding belief states in (a) 1D, (b) 2D, and (c) 3D. The belief state, which consists of the agent's location (depicted by a black dot) and of a discrete probability distribution over the possible source locations, encodes all past observations made by the agent (the agent's initial position is shown by a cross in observation maps). In (c), the source probability distribution is shown in cut-off planes containing the agent.

the agent location \mathbf{x}_0^a is at the center of the domain and where the prior distribution of source location $p_0(\mathbf{x})$ is drawn randomly from the set of priors (details are provided in Section II F 1).

- The source location \mathbf{x}^s is drawn randomly according to $p_0(\mathbf{x})$.

- At the t^{th} step of the search
 1. Knowing the current belief state $s_t = [\mathbf{x}_t^a, p_t(\mathbf{x})]$, the agent chooses an action according to some policy π : $a_t = \pi(s_t)$.
 2. The agent moves deterministically to the neighbor cell associated to a_t , perceives a unit cost and its position is updated to \mathbf{x}_{t+1}^a .
 3. The agent receives an observation o_t and the source location distribution is updated, using Bayes' rule, to $p_{t+1}(\mathbf{x}) = \text{Bayes}(p_t(\mathbf{x}), \mathbf{x}_{t+1}^a, o_t)$ (the Bayes operator will be made explicit in Section II D).
 - 3a. If $s_{t+1} = s^\Omega$, the search terminates and the agent perceives no more costs.
 - 3b. Otherwise, the search continues.

Each episode (each search) is a sequence like this:

$$s_0, a_0, o_0, s_1, a_1, o_1, \dots, s_{T-1}, a_{T-1}, o_{T-1}, s^\Omega$$

and the cumulated cost of an episode is equal to the number of steps T to termination (which can be infinite if the source is never found). A step-by-step illustration depicting how a search proceeds is provided in Supplemental Material.

The performance of a policy π is measured by $\mathbb{E}_{p_0, \pi}[T]$, the expected number of steps to reach the source, where the expectation is over all possible sequences generated following policy π , and over all possible priors p_0 (and, implicitly, over all possible source locations, which are distributed according to these priors). The optimal policy is the policy that minimizes $\mathbb{E}_{p_0, \pi}[T]$. We expand on the optimal policy in the next section.

Since the search does not stop until the source is found, any policy that fails to ensure termination with probability one has an infinite cumulated cost. While it is trivial to show that a policy which guarantees termination exists (any policy that exhaustively searches the grid), the policies we will consider (including infotaxis) do not have such guarantee. Therefore we will evaluate the performance of a policy based on (i) the probability of failure (never finding the source), which must approach zero, and (ii) the mean number of steps to reach the source, provided that the source is ultimately found.

B. Optimal policy

Solving the source-tracking problem means finding the optimal policy π^* that minimizes the duration of the

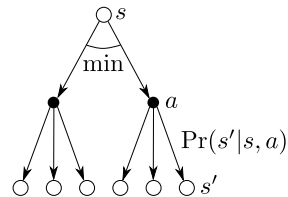


FIG. 3. Backup diagram for the optimal value function (using the notation conventions of ref. [15]).

search

$$\pi^* = \arg \min_{\pi} \mathbb{E}_{p_0, \pi}[T]. \quad (1)$$

The optimal policy can, at least formally, be determined from the solution of a recurrence equation known as the optimal Bellman equation as follows.

The optimal value function $v^*(s)$ of a belief state s is defined as the minimum, over all policies, of the expected number of steps remaining to find the source when starting from belief state s . It satisfies the optimal Bellman equation:

$$v^*(s) = \min_a \sum_{s'} \Pr(s'|s, a)[1 + v^*(s')] \quad \forall s \neq s^\Omega \quad (2)$$

where $\Pr(s'|s, a)$ is the probability of transitioning from belief state s to next belief state s' after executing action a , and where $v^*(s^\Omega) = 0$ (by definition of the terminal state s^Ω). Possible transitions from s to s' corresponds to possible observations: either finding the source (F) or not finding the source (\bar{F}) and receiving h hits. A visual explanation is provided in Fig. 3.

Given $v^*(s)$, the optimal policy consists in choosing the action that minimizes the expected number of remaining steps $v^*(s')$:

$$\pi^*(s) = \arg \min_a \sum_{s'} \Pr(s'|s, a)[1 + v^*(s')]. \quad (3)$$

When the number of states s is finite (and small enough), Eq. (2) can be solved using dynamic programming [15, 31]. In the source-tracking problem however, s contains a discrete probability distribution, of which there are infinitely many. More precisely, there are as many belief states as there are possible histories (sequences of actions and observations, which can be infinitely long). Even if a maximum duration t_{\max} were imposed, the number of possible beliefs grows as $(A \times O)^{t_{\max}}$ where O is the number of possible observations (at least 3) and A is the number of possible actions (twice the number of dimensions). To take an example, consider a 2D domain of 10 by 10 cells: with $A = 4$, $O = 3$, and $t_{\max} = 100$, the number of possible beliefs is larger the number of atoms in the observable universe. Therefore the optimal policy is, in general, not computable. It can, however, be well approximated: we will come back to this in Section V.

A lower bound for $\mathbb{E}_{p_0, \pi^*}[T]$ can be obtained by considering an omniscient agent that has access to the source

location. In that case the optimal policy is simply to follow the shortest path to the source, and T is the Manhattan distance $\|\mathbf{x}^s - \mathbf{x}^a\|_1$ between the agent and the source. The lower bound is obtained by taking the expectation of T over the initial source distribution:

$$\mathbb{E}_{p_0, \pi^*}[T] \geq \mathbb{E}_{p_0} \left[\sum_{\mathbf{x}} p_0(\mathbf{x}) \|\mathbf{x} - \mathbf{x}_0^a\|_1 \right] \quad (4)$$

Note that this lower bound is not tight since it assumes full observability, however it should be approached as the rate of information received by the agent increases.

An upper bound for $\mathbb{E}_{p_0, \pi^*}[T]$ can be obtained by considering an agent without sensors (no information provided by hits) that searches the domain exhaustively following a predetermined trajectory. The optimal trajectory in this scenario is an optimization problem on its own [32], however a simple yet efficient way to cover space is by “spiraling” outward from the starting point (visiting all cells within a Chebyshev distance d of the agent’s initial position, then covering all cells at a distance $d+1$, and so on, avoiding as much as possible visiting the same cell twice). In 1D, such spirals are not efficient (the constant back-and-forth motion of the agent would result in a quadratic scaling of the search time with the domain size). An alternative simple trajectory consists in going to one end of the grid and then to the other end. In either case, we call this policy $\pi^{\text{exhaustive}}$ and we can write

$$\mathbb{E}_{p_0, \pi^*}[T] \leq \mathbb{E}_{p_0, \pi^{\text{exhaustive}}}[T] = \sum_{\mathbf{x}} p_0(\mathbf{x}) r(\mathbf{x}) \quad (5)$$

where $r(\mathbf{x})$ is the time step at which location \mathbf{x} is visited following the prescribed trajectories (the first visited cell corresponds to $r = 1$, the next one to $r = 2$, etc.).

C. Probabilistic model of detections

We now need to specify the model used to generate observations (hits), that is, to specify $\Pr(h|\mathbf{x}^a, \mathbf{x}^s)$. This model is based on a physical modeling of dispersion and detection in a turbulent medium as follows.

The source emits detectable odor particles with a finite lifetime which disperse in the ambient turbulent environment and can be detected by the searcher. The detection events, or “hits”, are distributed according to a Poisson’s law

$$\Pr(h|\mu) = \frac{\mu^h \exp(-\mu)}{h!} \quad (6)$$

where μ is the mean number of hits. Physically, μ is a mean flux of odor particles toward the agent. It is a function of the Euclidean distance $d = \|\mathbf{x}^s - \mathbf{x}^a\|_2$ between the agent and the source (and of the physical parameters that govern detection and dispersion, they are described

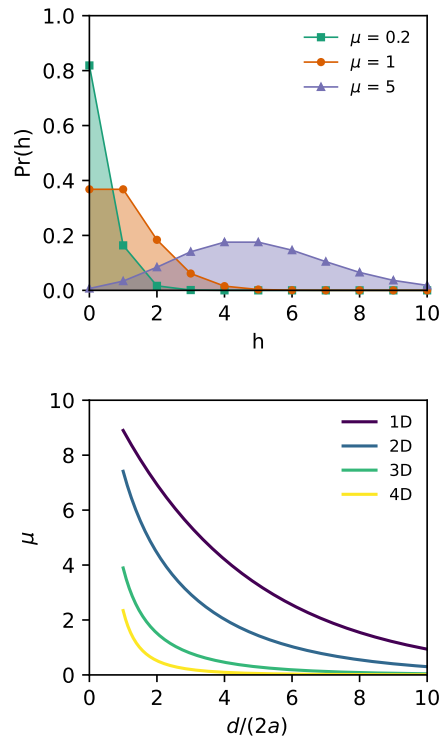


FIG. 4. Illustration of the detection model: hits h are distributed according to a Poisson’s law parameterized by its mean μ , which is a decreasing function of the Euclidean distance d to the source, and which functional form depends on the problem dimensionality (here $\lambda/a = 8$ and $R\Delta t = 10$).

in the next paragraph). Therefore $\Pr(h|\mathbf{x}^a, \mathbf{x}^s)$ is simply

$$\Pr(h|\mathbf{x}^a, \mathbf{x}^s) = \Pr(h|\mu(d)) \text{ with } d = \|\mathbf{x}^s - \mathbf{x}^a\|_2. \quad (7)$$

The derivation of $\mu(d)$ for an arbitrary number of dimensions n is detailed in Appendix A. The resulting expressions are provided below:

$$n = 1 : \quad \mu(d) = R\Delta t \frac{\lambda}{\lambda - a} \exp(-d/\lambda) \quad (8a)$$

$$n = 2 : \quad \mu(d) = R\Delta t \frac{1}{\ln(\lambda/a)} K_0(d/\lambda) \quad (8b)$$

$$n = 3 : \quad \mu(d) = R\Delta t \frac{a}{\lambda} \frac{\lambda}{d} \exp(-d/\lambda) \quad (8c)$$

$$n = 4 : \quad \mu(d) = R\Delta t \left(\frac{a}{\lambda}\right)^2 \frac{\lambda}{d} K_1(d/\lambda) \quad (8d)$$

and more generally for $n \geq 3$

$$\mu(d) = R\Delta t \left(\frac{a}{\lambda}\right)^{n-2} \left(\frac{\lambda}{d}\right)^{n/2-1} \frac{(n-2) K_{n/2-1}(d/\lambda)}{\Gamma(n/2) 2^{n/2-1}} \quad (8e)$$

where a is the agent radius, λ is the dispersion lengthscale of the particles in the medium, R is the source emission rate, Δt is the duration of a sensor measurement, Γ is the gamma function, and K_ν is the modified Bessel function

of the second kind of order ν . Note that we recover the expressions provided by [5] for $n = 2$ and $n = 3$. Examples of hit distributions and their mean as a function of the distance to the source are shown in Fig. 4.

D. Update by Bayesian inference

Each observation provides some information about the source location, which can be accounted for using Bayesian inference. In the case of a sequential process such as ours, Bayes' rule can be applied after each observation to maintain an up-to-date belief $p(\mathbf{x})$ which encompasses all information gathered so far. The update after observing o_t in \mathbf{x}_{t+1}^a reads

$$p_{t+1}(\mathbf{x}) = \text{Bayes}(p_t(\mathbf{x}), \mathbf{x}_{t+1}^a, o_t) \quad (9)$$

where $\text{Bayes}(p(\mathbf{x}), \mathbf{x}^a, o)$ is the operator that maps the prior p_t to the posterior p_{t+1} through Bayes' rule

$$\text{Bayes}(p(\mathbf{x}), \mathbf{x}^a, o) = \frac{\text{Pr}(o|\mathbf{x}^a, \mathbf{x})p(\mathbf{x})}{\sum_{\mathbf{x}'} \text{Pr}(o|\mathbf{x}^a, \mathbf{x}')p(\mathbf{x}')} \quad (10)$$

and where $\text{Pr}(o|\mathbf{x}^a, \mathbf{x})$ is called the evidence in Bayesian terminology.

Let's now go through the update rule for each observation. If $o = F$, the source has been found in \mathbf{x}^a , and the posterior distribution is simply a Dirac distribution

$$\text{Bayes}(p(\mathbf{x}), \mathbf{x}^a, F) = \delta(\mathbf{x} - \mathbf{x}^a). \quad (11)$$

Otherwise, $o = (\bar{F}, h)$, signifying that the source has not been found and that h hits were received. The posterior distribution after not finding the source a simple renormalization

$$\text{Bayes}(p(\mathbf{x}), \mathbf{x}^a, \bar{F}) = \begin{cases} 0 & \text{if } \mathbf{x} = \mathbf{x}^a, \\ \frac{p(\mathbf{x})}{\sum_{\mathbf{x} \neq \mathbf{x}^a} p(\mathbf{x})} & \text{otherwise.} \end{cases} \quad (12)$$

The posterior after a hit h is

$$\text{Bayes}(p(\mathbf{x}), \mathbf{x}^a, h) = \frac{\text{Pr}(h|\mathbf{x}^a, \mathbf{x})p(\mathbf{x})}{\sum_{\mathbf{x}'} \text{Pr}(h|\mathbf{x}^a, \mathbf{x}')p(\mathbf{x}')}. \quad (13)$$

The full update after observing $o = (\bar{F}, h)$ is therefore given by the successive application of each partial update

$$\text{Bayes}(p(\mathbf{x}), \mathbf{x}^a, o) = \text{Bayes}(\text{Bayes}(p(\mathbf{x}), \mathbf{x}^a, \bar{F}), \mathbf{x}^a, h). \quad (14)$$

A step-by-step illustration of Bayesian updates performed during a search is provided in Supplemental Material.

E. Parameters of the problem

The discrete source-tracking problem is parameterized by:

1. the space resolution Δx (the size of the agent's step, also the linear size of a grid cell);
2. the time resolution Δt (how often does the agent make a decision, also the integration time for the sensors); or alternatively the agent speed v and then $\Delta t = \Delta x/v$;
3. the probabilistic law for hits encounters, itself parameterized by $(a, \lambda, R, \Delta t)$, where a is the agent's radius, λ is the characteristic lengthscale of dispersion, R is the source emission rate;
4. the initial conditions (prior source distribution and agent's position);
5. the grid size (linear size of the domain) N .

The number of parameters can be greatly reduced by assuming that the search is initialized by a (nonzero) hit. The advantages are twofold: (i) the definition of the start is not arbitrary but instead corresponds to the moment when the agent is informed that there is source (as opposed to nothing) in the neighborhood and where tracking it down becomes meaningful, and (ii) the grid size can be chosen large enough such that the domain boundaries play virtually no role in the search because the prior distribution after a hit decays exponentially with the distance to the agent (mimicking an open world is highly desirable since the physical problem of dispersion is modeled for an infinite space and any finite-size effect in this context would be physically irrelevant). The details of this initialization procedure are provided in Section III F 1. We will also assume that the size of the agent step is equal to its body diameter $\Delta x = 2a$.

With this protocol, the source-tracking problem involves only four parameters which govern the physics of propagation and detection ($\Delta x, \lambda, R, \Delta t$). From those we can construct two independent dimensionless numbers, we chose

$$\mathcal{L} = \frac{\lambda}{\Delta x} \quad \text{and} \quad \mathcal{I} = R\Delta t \quad (15)$$

which characterize the problem size the source intensity, respectively. The dimensionless performance of the agent is measured in terms of the number of steps T to find the source, which can be converted back into a distance traveled ($T\Delta x$) or a time elapsed ($T\Delta t$).

F. Methods

1. Initialization protocol

The physical problem of source-tracking and its modeling assumes an infinite, open domain. Because tracking can only start once the searcher knows that a source exists, i.e. after a detection event occurred, we propose to start the search with a nonzero hit and give a criteria to

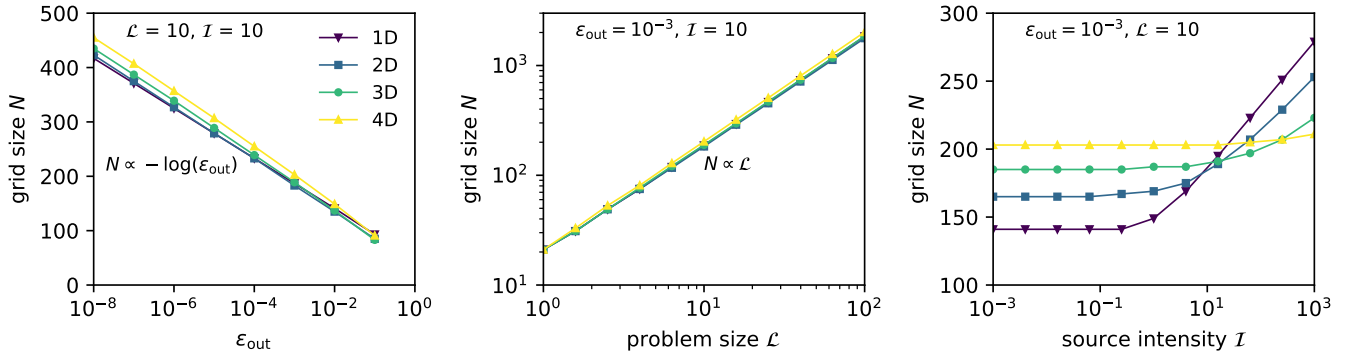


FIG. 5. Initialization procedure: grid size as a function of ε_{out} , $\mathcal{L} = \lambda/\Delta x$ and $\mathcal{I} = R\Delta t$ when following our methodology.

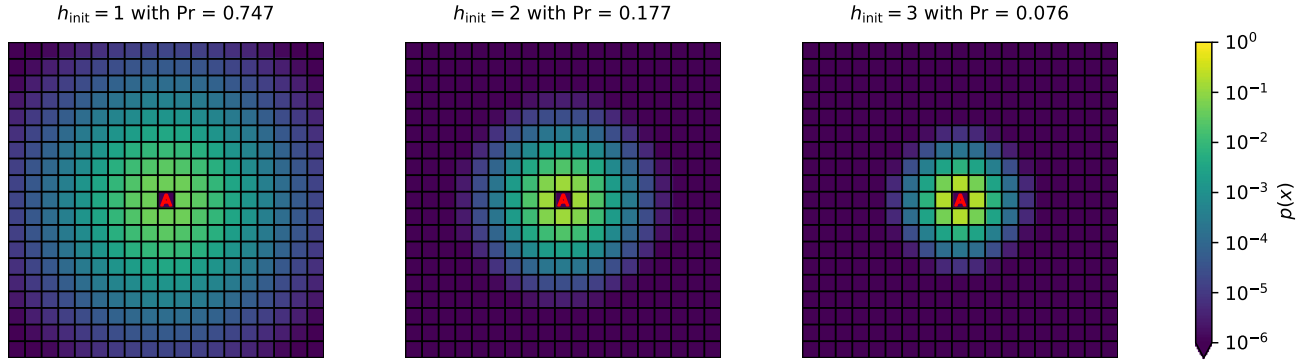


FIG. 6. Initialization procedure: a set of initial beliefs p_0 , here in 2D for $\mathcal{L} = 1$ and $\mathcal{I} = 2$, with the corresponding probabilities of occurring and the value of the initial hit shown on top. “A” indicates the agent’s position, at the center of the domain.

define a numerical domain “large enough” to mimic an open domain.

To simplify the derivation we will assume in the following a continuous space. Consider a spherical coordinates system (in n dimensions) centered on the agent. We denote $\Pr(r)dr$ the probability of the source being in a spherical shell of radius r and thickness dr . Before the search starts, we assume a uniform prior over the entire domain and excluding the agent’s volume:

$$\Pr(r) = \begin{cases} 0 & \text{for } r \in [0, a] \\ cS(r) & \text{for } r > a \end{cases} \quad (16)$$

where a is the agent’s radius, c is a constant and $S(r)$ is the surface area of the n -ball of radius r . After a initial hit h_{init} , using Bayes’ rule, we can write

$$\Pr(r|h_{\text{init}}) = \frac{\Pr(h_{\text{init}}|r) \Pr(r)}{\Pr(h_{\text{init}})} \quad \text{for } r > a \quad (17)$$

with the normalization constant given by

$$\Pr(h_{\text{init}}) = \int_a^\infty \Pr(h_{\text{init}}|r) \Pr(r) dr. \quad (18)$$

For $h_{\text{init}} \neq 0$, $\Pr(r|h_{\text{init}})$ decays exponentially fast with r for large r . We can define a cut-off radius R_c such that

the probability of the source being outside a ball of radius R_c is at most ε_{out} for any h_{init} (with ε_{out} small). This reads

$$R_c = \max_{h_{\text{init}} \neq 0} r_c(h_{\text{init}}) \quad (19)$$

where $r_c(h_{\text{init}})$ is implicitly defined by

$$\int_a^{r_c(h_{\text{init}})} \Pr(r|h_{\text{init}}) dr = 1 - \varepsilon_{\text{out}}. \quad (20)$$

The initialization procedure for the search is therefore as follows.

1. The initial hit h_{init} is drawn at the beginning of each episode from the corresponding probability distribution (excluding zero hit):

$$\Pr(h_{\text{init}}|h_{\text{init}} \neq 0) = \begin{cases} 0 & \text{if } h_{\text{init}} = 0 \\ \Pr(h_{\text{init}})/Z & \text{otherwise} \end{cases} \quad (21)$$

with Z the normalization constant such that $\sum_{h_{\text{init}}} \Pr(h_{\text{init}}|h_{\text{init}} \neq 0) = 1$.

2. The linear size of the grid, N , is set to

$$N = 2 \text{ceil}(R_c) + 1. \quad (22)$$

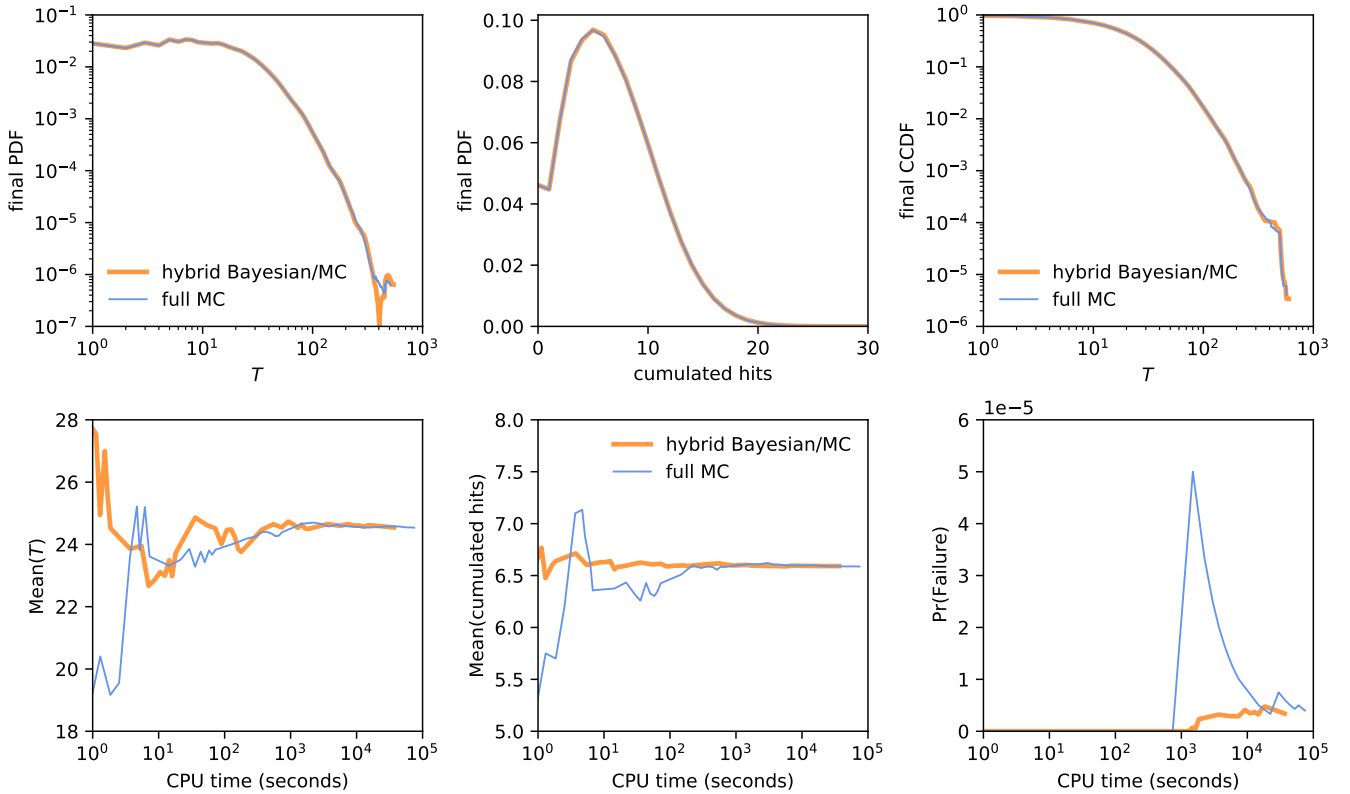


FIG. 7. Comparison of full Monte-Carlo and hybrid Bayesian/Monte-Carlo methods (here with $\varepsilon_{\text{stop}} = 10^{-10}$) for computing the statistics of a policy: both methods ultimately yield the same distributions (top row), but the hybrid method converges faster and is well-suited for probing rare events, such as the probability of never finding the source with the infotaxis policy (bottom row). PDF stands for probability density function (which shows the probability of finding the source in T steps), and CCDF stands for complementary cumulative distribution function (which shows the probability of the source not being found after T steps). The number of cumulated hits does not include the initial hit used to define the start of the search. A total of 10^6 and 2×10^5 episodes were used for the full Monte-Carlo and the hybrid Bayesian/Monte-Carlo methods, respectively. These simulations used the infotaxis policy in 2D with $\mathcal{L} = 2$ and $\mathcal{T} = 2$.

This methodology essentially yields $N \propto \mathcal{L}$ with a proportionality constant that depends on ε_{out} (and weakly on \mathcal{T}), as shown in Fig. 5.

3. The source distribution is set to uniform: $p_{\text{init}}(\mathbf{x}) = 1/N^n$
4. The agent's position \mathbf{x}_0^a is set to the center of the domain
5. The initial source distribution p_0 is computed using $p_0 = \text{Bayes}(p_{\text{init}}(\mathbf{x}), \mathbf{x}_0^a, (\bar{F}, h_{\text{init}}))$, and the initial belief state is then $s_0 = [\mathbf{x}_0^a, p_0(\mathbf{x})]$.

Following this procedure, the set of initial beliefs p_0 is the set generated by $h_{\text{init}} = \{1, 2, \dots\}$ and their probabilities of occurring are given by Eq. (21). An example of such a set is shown in Fig. 6.

2. Policy evaluation

Policy evaluation is performed by generating a large number of episodes and computing the resulting distri-

bution of arrival times T , denoted here $f(T)$, and defined such that its norm is the probability of (ever) finding the source (which may not be equal to one), that is,

$$\Pr(\text{failure}) = 1 - \sum_T f(T). \quad (23)$$

Other moments of the distribution are computed after renormalization as usual. The normalized distribution is

$$\tilde{f}(T) = \frac{f(T)}{\sum_T f(T)} \quad (24)$$

and we have

$$\text{Mean}(T) = \sum_T T \tilde{f}(T) \quad (25)$$

and

$$\text{Std}(T) = \sqrt{\sum_T T^2 \tilde{f}(T) - \text{Mean}(T)^2}. \quad (26)$$

The convergence of $f(T)$ with the number of episodes can be vastly improved by realizing that $p(\mathbf{x})$, interpreted as the agent’s belief in the context of decision-making, is also the true (in the Bayesian sense) probability distribution of sources that could have generated the sequence of observations. In this probabilistic approach, each episode can be continued until the probability of having found the source is equal to one (within numerical accuracy $\varepsilon_{\text{stop}}$) or until the agent is stuck in an infinite loop, and the hits are drawn at each step according to the distribution:

$$\Pr(h|\mathbf{x}^a) = \sum_{\mathbf{x}} \Pr(h|\mathbf{x}^a, \mathbf{x})p(\mathbf{x}) \quad (27)$$

such that episodes can be generated independently of the true source location \mathbf{x}^s . We refer to this alternative framework as “hybrid Bayesian/Monte-Carlo” (as opposed to “full Monte-Carlo”). More details about its implementation are given in Appendix B 1, and the numerical proof of its correctness and efficiency is given in Fig. 7. An video illustrating how the search proceeds in this framework is also provided in Supplemental Material. This approach is particularly advantageous to sample rare events (such as failing to find the source) and more generally to sample heavy-tailed distributions (as is $f(T)$). Besides, Eq. (27) can be viewed as a tensor dot product, and can be computed efficiently by storing $\Pr(h|\mathbf{x}^a, \mathbf{x})$ for all possible values of h beforehand (see Section II F 3 for more details).

The number of episodes is chosen such that the mean of the distribution is well-converged (95% confidence interval less than $\pm 2\%$). Typically we use at least 16000 episodes in 1D, 6400 episodes in 2D, and 25600 episodes in 3D. In 4D, we determined the mean with less accuracy due to the high cost of the simulations: we used typically 4096 episodes (yielding a 95% confidence interval less than $\pm 10\%$) and down to 1024 episodes for the most expensive cases.

3. Numerical implementation

The code we used is open-source and freely available [the code will be released upon acceptance]. Important details of our implementation, in particular the chosen values of numerical parameters, are reported in Table I and discussed in this section.

For ε_{out} , which determines the grid size in the initialization protocol (Section II F 1), we used $\varepsilon_{\text{out}} = 10^{-3}$. This particular value of ε_{out} was determined from preliminary tests showing that the mean time to find the source with the infotaxis policy has converged to a constant independent of ε_{out} for $n > 1$ (as we shall see, in 1D and in the absence of hits, infotactic agents tend to go to one end of the domain before turning back, therefore the mean time to find the source does not converge with the domain size).

For $\varepsilon_{\text{stop}}$, which is required by the Bayesian/Monte-Carlo setting, we used $\varepsilon_{\text{stop}} = 10^{-6}$: this means that the

dimension	ε_{out}	$\varepsilon_{\text{stop}}$	ε_{acc}	N_{stuck}	number of episodes
1D	10^{-3}	10^{-6}	10^{-10}	8	≥ 16000
2D	10^{-3}	10^{-6}	10^{-10}	8	≥ 6400
3D	10^{-3}	10^{-6}	10^{-10}	8	≥ 25600
4D	10^{-3}	10^{-6}	10^{-10}	8	[1024,4096]

TABLE I. Summary of numerical parameters used to compute statistics: ε_{out} determines the size of the numerical domain, $\varepsilon_{\text{stop}}$ defines the stopping criteria in the Bayesian/Monte-Carlo approach, ε_{acc} is the numerical accuracy used to determine whether two actions are equivalent, and N_{stuck} provides a criteria to declare that the agent is stuck in an infinite loop.

search continues until the probability that the source has not been found is less than 10^{-6} . We found that this value was sufficiently low to obtain very clean statistics of the arrival times (in particular of the tail of their distribution) while keeping the computational cost acceptable.

Besides, one must choose an upper limit for the hit values h , since parts of the computations involve a summation over h . We recall (cf. Section II C) that h is a random variable following a Poisson distribution with mean (and variance) $\mu(d)$ where μ is a decreasing function of the distance d between the agent and the source. A natural way to compute a summation over h would consist in keeping adding terms associated to increasing values of h until the desired accuracy is reached. However, for computational efficiency, we found desirable to set this cut-off value to a constant (independent of the distance to the source). The cut-off value for h was set to $\text{Mean}(h) + \text{Std}(h)$ at a distance Δx from the source, that is

$$h_{\text{max}} = \mu(\Delta x) + \sqrt{\mu(\Delta x)}. \quad (28)$$

Note that $d = \Delta x$ is the minimal distance between the agent and the source (μ is not defined for $d = 0$ since this would mean that the source is found). We ensured that this cut-off value was large enough not to affect our results.

Finally, even with deterministic policies, the choice of action is not unique in case of ties. Consider for example the choice of the first action: all actions are equivalent due to the symmetries of the problem. However, due to finite numerical accuracy, these symmetries may be broken artificially. On the other hand, numerical accuracy can generate artificial ties later in the search. Consider for example the infotaxis policy which consists in choosing the action that minimizes the expected entropy of the next belief state (a complete description of infotaxis will be provided in Section III). Close to the end of the search, the entropy may be very low, and numerically indistinguishable from zero, leading to “wrong” choices. To ensure reproducibility of our results, we control the numerical accuracy by introducing a small parameter ε_{acc} . We assume that two actions are equivalent if the criteria used by the policy to evaluate them (for example the expected entropy for infotaxis or the expected optimal value

for the optimal policy) are equal within $\varepsilon_{\text{acc}} = 10^{-10}$.

Common practice consists in breaking ties randomly. Here we chose instead to break ties in a deterministic manner: when 'left' and 'right' are equivalent, the chosen action will always be 'left'. This allows us to easily identify situations where the agent is lost (in the sense that the policy can no longer discriminate between actions, for example because the agent ventured too far from the source): with our setup, a lost agent will be trapped in an infinite loop which is trivial to detect and allows us to stop the simulation. In contrast, with random tie-breaking, a lost agent would perform a random walk, which is of no interest for the problem we consider and would waste huge computational resources (think how long it takes to a random walk to explore a 4D space).

Rigorously speaking, infinite loops in the agent's displacements may not be truly infinite, since they may be broken by a lucky hit if one waits long enough. These finite loops essentially amount to waiting for such a lucky hit to happen, and their presence always degrade performance, therefore we declare the agent as stuck and stop the search when a "long enough" loop is encountered. More precisely, the agent is stuck if $\mathbf{x}_t^a = \mathbf{x}_{t-2}^a$ more than N_{stuck} times in a row. We used $N_{\text{stuck}} = 8$ in our simulations. The particular choice of N_{stuck} has no effect on the performance we report for good policies such as infotaxis and its derivatives, since they are not prone to such loops. It may however affect our measure of performance for policies which systematically generates loops (such as those presented in Section II G). It is unimportant though, since such policies are always poor.

G. Source-tracking is hard

To get a sense of the difficulty of the source-tracking problem, it is worth reporting the performance of simple (and somewhat naive) heuristic policies, including some proposed for robotic navigation by Cassandra et al. [16]. We recall that the policy is a mapping from belief state s to action a , where the belief state is $s = [\mathbf{x}^a, p(\mathbf{x})]$ with \mathbf{x}^a the agent's position and $p(\mathbf{x})$ the probability distribution of source locations. For each possible action corresponds a new deterministic position which we denote $\mathbf{x}^a(a)$.

We first consider the usual "greedy" policy, defined as the short-sighted exploitative policy that minimizes the penalty at the next step. In the source tracking problem, the greedy policy consists in choosing the action which maximizes the probability of finding the source in the next cell:

$$\pi^{\text{greedy}}(s) = \operatorname{argmax}_a p(\mathbf{x}^a(a)). \quad (29)$$

The probability of failure with the greedy policy is plotted in Fig. 8(a) for 2D searches. In the absence of cues ($\mathcal{I} \rightarrow 0$), the greedy policy performs well because it behaves as an exhaustive search, spiraling outward from the

center of the domain. However in the presence of cues the greedy agent is often lost, with $\Pr(\text{failure})$ greater than 1 % or even 10 %. This is due to the locality of the greedy policy (the greedy agent chooses its action based only on $p(\mathbf{x})$ around itself) which tends to trap the agent in a neighborhood of vanishing $p(\mathbf{x})$ from where it cannot escape. Videos illustrating the behavior of the greedy policy are available in Supplemental Material.

We then consider three policies that would be optimal in the absence of uncertainty, since they would all direct the agent to the (known) source location.

The first one is the "most likely state (mls)" policy [16] which finds the most likely source location, and executes the action that would be optimal for that location. In other words, the agent executing this policy moves in the direction of the most likely source location. This reads

$$\pi^{\text{mls}}(s) = \operatorname{argmin}_a \|\mathbf{x}^{\text{mls}} - \mathbf{x}^a(a)\|_1 \quad (30)$$

where \mathbf{x}^{mls} is the most likely source location

$$\mathbf{x}^{\text{mls}} = \operatorname{argmax}_{\mathbf{x}} p(\mathbf{x}). \quad (31)$$

Another possibility is the "voting" policy [16] which chooses the action that is the most likely to be optimal. For that, it determines the optimal action for each possible source location, weights each action by the corresponding probability of that location, and picks the the action with the highest probability. The probability that action a is optimal is

$$w(a) = \sum_{\mathbf{x}} \Pr(\mathbf{x}) \phi(a^*(\mathbf{x}) = a) \quad (32)$$

where ϕ has value 1 if the argument is true and 0 otherwise, and where $a^*(\mathbf{x})$ denote the optimal action for a source located in \mathbf{x} , which is given by

$$a^*(\mathbf{x}) = \operatorname{argmin}_a \|\mathbf{x} - \mathbf{x}^a(a)\|_1. \quad (33)$$

The voting policy then reads

$$\pi^{\text{voting}}(s) = \operatorname{argmax}_a w(a). \quad (34)$$

We finally consider a policy based on the intuitive idea that the agent should get, on average, closer to the source. For a belief state $s = [\mathbf{x}^a, p(\mathbf{x})]$, the mean distance to the source is denoted D and defined by

$$D(s) = \sum_{\mathbf{x}} p(\mathbf{x}) \|\mathbf{x} - \mathbf{x}^a\|_1. \quad (35)$$

where we used the Manhattan norm (other norms would yield similar results). The expected value of this mean distance upon executing action a in belief state s is given by

$$D(s|a) = \sum_{s'} \Pr(s'|s, a) D(s') \quad (36)$$

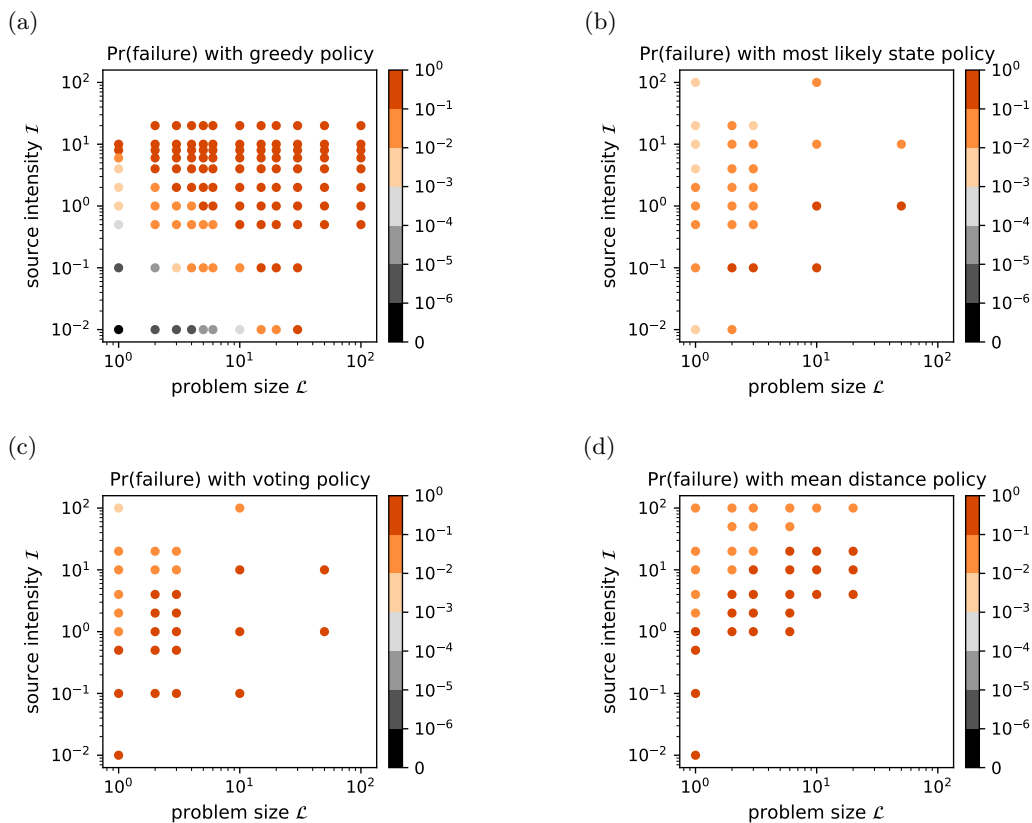


FIG. 8. Source-tracking is hard: probability of never finding the source in 2D for (a) the greedy policy, (b) the most likely state policy, (c) the voting policy and (d) the mean distance policy, as a function of the problem size $\mathcal{L} = \lambda/\Delta x$ and source intensity $\mathcal{I} = R\Delta t$.

where the sum is taken over all successor belief states s' . The “mean distance” policy is then defined by

$$\pi^{\text{mean distance}}(s) = \underset{a}{\operatorname{argmin}} D(s|a) \quad (37)$$

and consists in choosing the action that minimizes the expected Manhattan distance to the source at the next step. Besides, for any belief state, the mean Manhattan distance is a lower bound for the optimal value $v^*(s)$:

$$D(s) \leq v^*(s). \quad (38)$$

The mean distance policy therefore minimizes the expected lower bound of the optimal value function.

The probabilities of failing to find the source in 2D with the most-likely-state, voting and mean-distance policies are shown in Fig. 8(b,c,d). Reliability is very poor for the entire range of parameters, with $\Pr(\text{failure})$ always greater than 0.1 %, and often larger than 1 % or even 10 %. This is because an agent following any of those policies gets systematically trapped in loops early on during the search. Videos illustrating the behavior of these different policies are provided in Supplemental Material.

These examples show that an agent following any of the simple heuristic policies presented in this section will easily miss the source and be lost. The greedy policy,

which is locally optimal, fails due to self-trapping. Policies that would be optimal in the absence of uncertainty are plagued by the emergence of loops. These loops are due to spatial symmetries in $p(\mathbf{x})$, which arise because of the absence of directionality in the information provided by hits. The reliability of infotaxis over the entire parameter range (which we will show in the next section) is therefore a feat far from trivial to achieve.

III. THE INFOTAXIS POLICY

Infotaxis [5] is a heuristic solution to the source-tracking problem which greedily minimizes uncertainty on the source location: at each step, an infotactic agent chooses the action that maximizes the expected reduction in entropy of the posterior belief. The idea of information maximization is natural for pure exploration tasks and has long been used in robotics under the name of “greedy exploration” [17]. It is, however, unclear why greedily accumulating information should minimize the cumulated cost in the source-tracking problem since the two are not linearly related (this can be easily verified numerically). In this section we describe the infotaxis policy and thoroughly evaluate its performance.

A. Description of infotaxis

The (Shannon) entropy of a belief state $s = [\mathbf{x}^a, p(\mathbf{x})]$ is defined by

$$H(s) = - \sum_{\mathbf{x}} p(\mathbf{x}) \log_2 p(\mathbf{x}) \quad (39)$$

and is a measure of how uncertain is the source location (we use the logarithm with base 2, as is standard in information theory where H is measured in bits of information). In particular, the entropy of a Dirac distribution is zero, so $H(s^\Omega) = 0$ (s^Ω is the terminal state where the source is found). Note that H is independent of the agent's position \mathbf{x}^a .

The expected entropy upon taking action a in belief state s , denoted $H(s|a)$, is the expected entropy of successor belief states s' :

$$H(s|a) = \sum_{s'} \Pr(s'|s, a) H(s') \quad (40)$$

where $\Pr(s'|s, a)$ is the probability of transitioning from belief state s to next belief state s' after executing action a .

The information gain associated with action a in belief state s is then given by

$$G(s, a) = H(s) - H(s|a) \quad (41)$$

Note that the information gain is also, by definition [33], the mutual information between the current belief state s and the possible observations after action a . The infotaxis policy, denoted $\pi^{\text{infotaxis}}$, consists in choosing the action that maximizes the information gain (or equivalently, the action that minimizes the expected entropy) at the next step, that is,

$$\pi^{\text{infotaxis}}(s) = \underset{a}{\operatorname{argmax}} G(s, a) = \underset{a}{\operatorname{argmin}} H(s|a). \quad (42)$$

Combining Eq. (40) with Eq. (42), the infotaxis policy can be written as

$$\pi^{\text{infotaxis}}(s) = \underset{a}{\operatorname{argmin}} \sum_{s'} \Pr(s'|s, a) H(s') \quad (43)$$

which makes clear that it shares the same structure as the optimal policy, given by Eq. (3) and which can be rewritten as

$$\pi^*(s) = 1 + \underset{a}{\operatorname{argmin}} \sum_{s'} \Pr(s'|s, a) v^*(s'). \quad (44)$$

If $v^*(s)$, the expected time to find the source starting from belief state s with the optimal policy, was a linear function of $H(s)$, then infotaxis would be optimal. A trivial counter-example shows that this is not the case: when the source location is known, v^* is equal to the Manhattan distance to the source whereas $H = 0$ for all source locations. It is also easy to check numerically that $H(s)$ and $v^{\text{infotaxis}}(s)$ (the expected remaining time to find the source starting from belief state s with the infotaxis policy) are not strongly linearly correlated, therefore $v^{\text{infotaxis}} \not\approx v^*$.

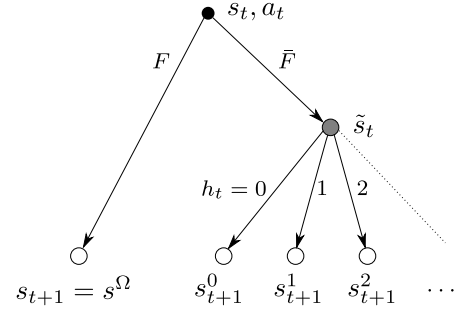


FIG. 9. Tree of possible successor belief states s_{t+1} starting from a belief state s_t and executing action a_t . Transitions from s_t to s_{t+1} are determined by the observations: either finding the source (F) or not finding the source (\bar{F}) and receiving h_t hits.

B. Explicit computation of the expected entropy

Let us consider an explicit example to show how $H(s|a)$ is calculated. Suppose that the agent is currently in belief state $s_t = [\mathbf{x}_t^a, p_t(\mathbf{x})]$, and consider an action a_t that would move the agent to a new position \mathbf{x}_{t+1}^a . Possible outcomes are

- with probability $p_t(\mathbf{x}_{t+1}^a)$, the agent will find the source and the new belief state will be s^Ω with $H(s^\Omega) = 0$,
- with probability $1 - p_t(\mathbf{x}_{t+1}^a)$, the agent will not find the source, and $p_t(\mathbf{x})$ is updated to $\tilde{p}_t(\mathbf{x}) = \text{Bayes}(p_t(\mathbf{x}), \mathbf{x}_{t+1}^a, \bar{F})$ (a simple renormalization to account for the absence of the source). We denote this intermediate belief state $\tilde{s}_t = [\mathbf{x}_{t+1}^a, \tilde{p}_t(\mathbf{x})]$. Then the agent will receive a hit h_t . Possible outcomes are:
 - the agent will receive 0 hit with probability $\Pr(h_t = 0 | \mathbf{x}_{t+1}^a)$, update the posterior to $p_{t+1}^0(\mathbf{x}) = \text{Bayes}(\tilde{p}_t(\mathbf{x}), \mathbf{x}_{t+1}^a, 0)$ and the new belief state will be $s_{t+1}^0 = [\mathbf{x}_t^a, p_{t+1}^0(\mathbf{x})]$ with entropy $H(s_{t+1}^0)$,
 - the agent will receive 1 hit with probability $\Pr(h_t = 1 | \mathbf{x}_{t+1}^a)$, and similarly the new belief state will be $s_{t+1}^1 = [\mathbf{x}_t^a, p_{t+1}^1(\mathbf{x})]$ with entropy $H(s_{t+1}^1)$,
 - etc.

as illustrated in Fig. 9. This gives

$$H(s_t|a_t) = p_t(\mathbf{x}_{t+1}^a) \cdot 0 + [1 - p_t(\mathbf{x}_{t+1}^a)] \left[\sum_{h_t} \Pr(h_t | \mathbf{x}_{t+1}^a) H(s_{t+1}^{h_t}) \right] \quad (45)$$

and where the probability of each hit value is computed from

$$\Pr(h_t | \mathbf{x}_{t+1}^a) = \sum_{\mathbf{x}'} \Pr(h_t | \mathbf{x}_{t+1}^a, \mathbf{x}') \tilde{p}_t(\mathbf{x}'). \quad (46)$$

C. Performance of infotaxis

In this subsection we provide a thorough assessment of the infotaxis policy. The performance of infotaxis has been evaluated in $n = \{1, 2, 3\}$ dimensions and for a wide range of problem sizes \mathcal{L} and source intensities \mathcal{I} (these dimensionless parameters are defined by Eq. (15)). A few additional simulations have also been performed in 4D. The results are summarized in Fig. 10 and Fig. 11. Missing data correspond to cases we cannot simulate, either because they require too much memory or because they are too expensive computationally. Videos showing infotactic searches are provided in Supplemental Material.

The first quantity of interest is the probability of failure, $\text{Pr}(\text{failure})$, which is plotted in the $(\mathcal{L}, \mathcal{I})$ plane in Fig. 10(a). In our simulations, we set $\varepsilon_{\text{stop}} = 10^{-6}$ therefore cases with $\text{Pr}(\text{failure}) \leq 10^{-6}$ have negligible probability of failure within our numerical accuracy (black dots). Conversely, cases with $\text{Pr}(\text{failure}) > 10^{-6}$ (grey to orange dots) exhibit a measurable probability of never finding the source, which is due to the agent getting stuck in an infinite loop at some point during the search (which then never terminates). It is clear from Fig. 10(a) that infotaxis does not always guarantee termination, however $\text{Pr}(\text{failure}) < 10^{-3}$ (black to grey shades) for almost all cases considered. The exceptions (orange shades) correspond to situations with small \mathcal{L} and large \mathcal{I} : these are searches where hits provide so much information that the source location can be identified exactly from a distance. In this situation, the entropy of the belief state is zero and cannot be reduced any further: the infotactic agent is then “lost”. This marginal issue could be easily fixed by requiring the agent to go to the source if its location is perfectly known.

The second quantity of interest is the mean number of steps to reach the source, provided that the source is found with sufficiently high probability (we set this threshold arbitrarily to 0.999). $\text{Mean}(T)$ is plotted in the $(\mathcal{L}, \mathcal{I})$ plane using a colormap in Fig. 10(b), where we also show grey contours for the mean cumulated number of hits (excluding the initial hit). A more quantitative representation of $\text{Mean}(T)$ is presented in Fig. 12, where we also show the theoretical lower and upper bounds we obtained for the optimal policy (computed according to Eqs. (4) and (5), respectively).

The upper bound was obtained by considering a search where the agent explores the space exhaustively by following n -dimensional spiralling trajectories, or, in 1D, by going to one end and then to the other end of the domain (unless the one-dimensional spiral is better, which is the case only for very small domains). This upper bound therefore scales as \mathcal{L}^n (with n the dimensionality), as illustrated by Fig. 12(a). Cases where $\text{Mean}(T)$ is larger than this upper bound are highlighted in Fig. 10(b) by outer circles: the mean search time achieved by infotaxis is never above the upper bound for the optimal policy, except in 1D for small \mathcal{L} and \mathcal{I} (a rather marginal con-

figuration).

Besides, it has been shown that in the absence of detections (succession of zero hits), infotactic trajectories are Archimedean spirals in 2D [5] and an approximate generalization of those in 3D [20, 22]. We recovered such trajectories, examples are shown in Fig. 13. However, in the 1D case, we found that infotaxis does not generate one-dimensional spirals but instead “end-to-end” trajectories in the absence of hits. These trajectories are essentially the ones we assumed to derive our upper bounds: the latter are therefore a very good estimate of $\text{Mean}(T)$ in the limit of no information $\mathcal{I} \rightarrow 0$, as can be seen from Fig. 12(b).

The lower bound was obtained by considering an agent which knows the source location, and hence scales linearly in \mathcal{L} . We expect the optimal policy to approach this bound when \mathcal{I} becomes large (though this bound is not tight). From Fig. 12(b), this is clearly the case for the infotaxis policy. Note that at high \mathcal{I} , infotactic agents tend to get stuck (cf. Fig. 10(a)), which limits the maximal value of \mathcal{I} we can reach.

Even though $\text{Mean}(T)$ is the quantity to minimize in the source-tracking problem, a strategy exhibiting huge fluctuations in search times may be too hazardous to be used in practice. We found that the standard deviation of the arrival times distribution, $\text{Std}(T)$, is of the same order of $\text{Mean}(T)$ with very little variations across the entire parameter range we explored: $\text{Std}(T)/\text{Mean}(T) \in [0.6, 1.1]$ in 1D, $[0.7, 1.9]$ in 2D, $[1.0, 2.7]$ in 3D, and around 3 in 4D (though the parameter range is very limited for the latter). The detailed data is provided in Fig. 11(b).

The distributions of arrival times for all considered parameters are presented in Fig. 14. It is worthwhile at this point to emphasize that compared to prior work, our methodology allowed us to properly sample the tail of the distributions up to $O(10)$ standard deviations. Our data (left column of Fig. 14) clearly establish that the tail is subexponential, unlike what was previously believed [5, 20, 28, 29]. It can also be verified, by plotting the same data using a log-log scale, that the tail decays faster than any power law (not shown). We found that the arrival time distributions approach log-normal distributions as the number of space dimension increases. The log-normal probability density function reads

$$f(T) = \frac{1}{\sigma\tau\sqrt{2\pi}} \exp\left(-\frac{(\ln T - \mu)^2}{2\sigma^2}\right) \quad (47)$$

where $\mu = \text{Mean}(\ln T)$ and $\sigma = \text{Std}(\ln T)$. The distribution of $\tau = (\ln T - \mu)/\sigma$ is plotted in Fig. 14 (right column). If T was perfectly log-normally distributed, τ would follow a standard normal distribution (which is shown by the dashed curve). Our results show that the log-normal distribution is a very good description for high-dimensional searches, and more generally of the tail of the distribution except maybe in the 1D case.

Log-normal distributions emerge as the statistical result of multiplicative random processes (in the limit of

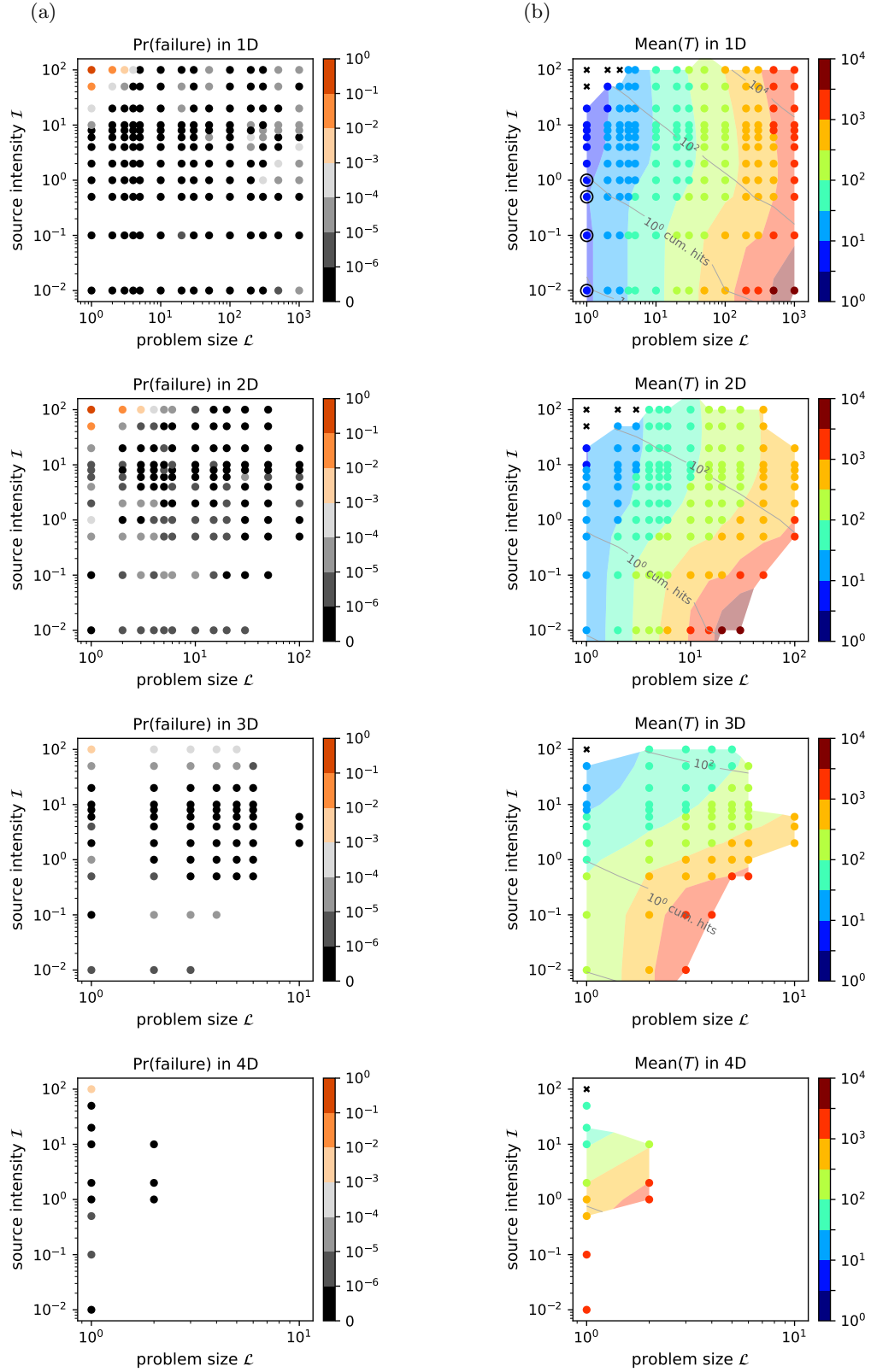


FIG. 10. Performance of infotaxis for source tracking in 1D, 2D, 3D and 4D (rows), for a wide range of physical parameters $\mathcal{L} = \lambda/\Delta x$ and $\mathcal{I} = R\Delta t$: (a) probability of never finding the source and (b) mean number of steps to find the source. In (b), the black crosses depict cases where $\text{Pr}(\text{failure}) > 10^{-3}$, the grey contour lines indicate the mean cumulated number of hits gathered along the search (the detailed data is shown in Fig. 11(a)), and the outer circles depict cases where $\text{Mean}(T)$ is larger than the upper bound we obtained for the optimal policy.

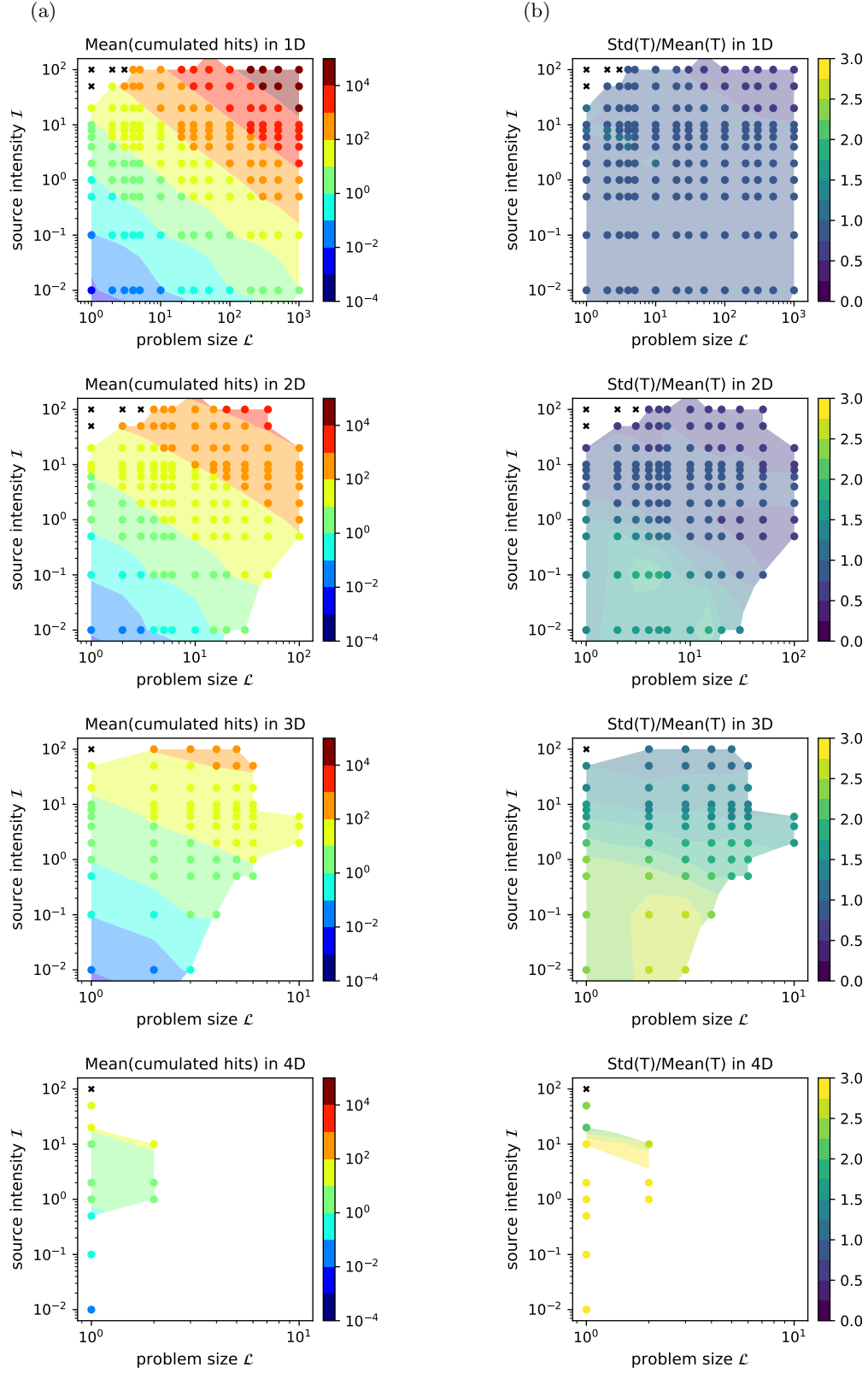


FIG. 11. Additional statistics of infotactic searches for source tracking in 1D, 2D, 3D and 4D (rows), for a wide range of physical parameters $\mathcal{L} = \lambda/\Delta x$ and $\mathcal{I} = R\Delta t$: (a) mean number of cumulated hits to find the source (excluding the initial one) and (b) standard deviation of arrival times distribution normalized by its mean. The crosses depict cases where $\text{Pr}(\text{failure}) > 10^{-3}$.

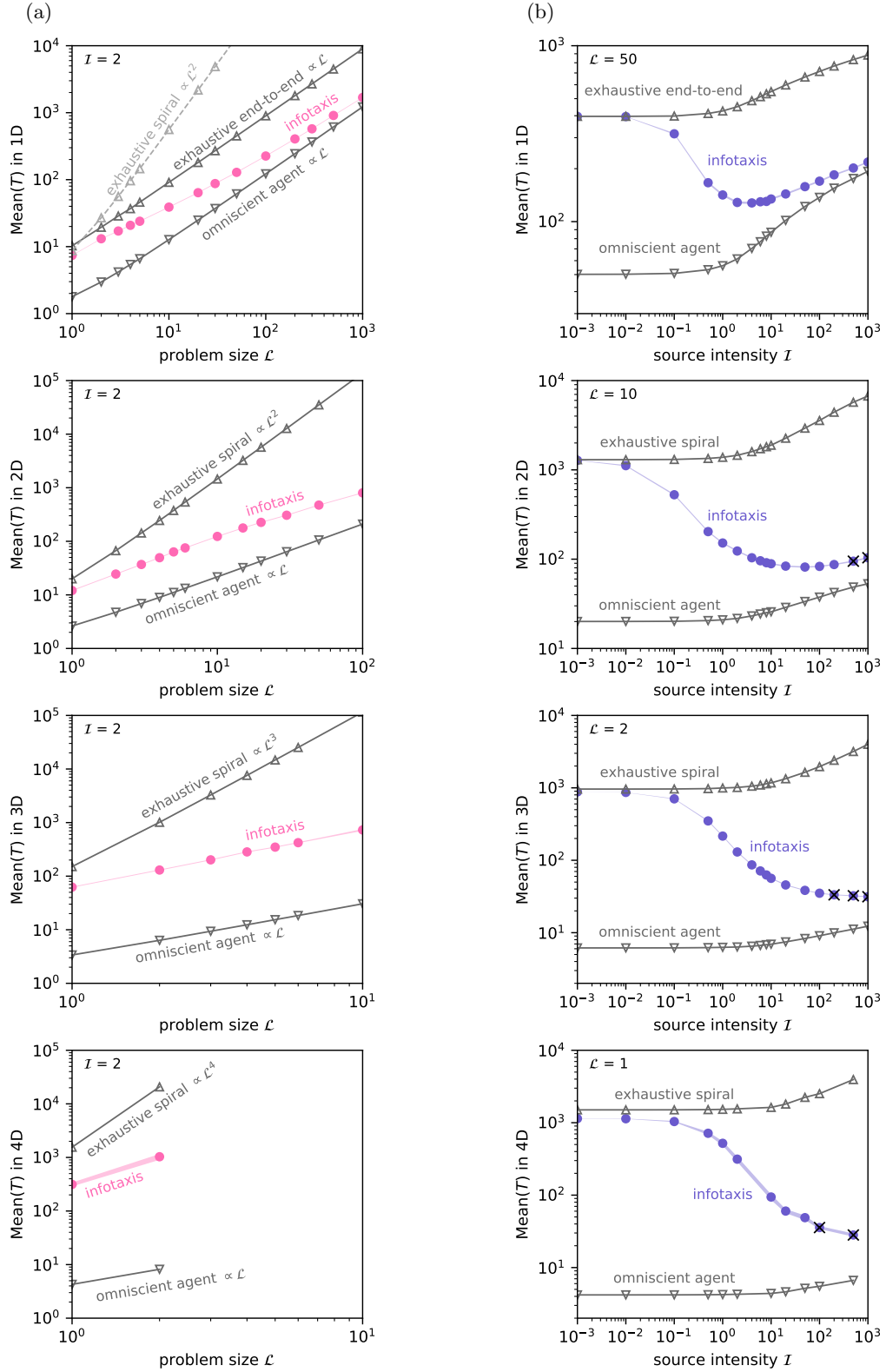


FIG. 12. Mean number of steps to find the source with infotaxis in 1D, 2D, 3D and 4D (rows) as a function of (a) the problem size $\mathcal{L} = \lambda/\Delta x$ and (b) the source intensity $\mathcal{I} = R\Delta t$. Infotaxis is depicted by dots (crossed dots indicate $\text{Pr}(\text{failure}) > 10^{-3}$), while downward (resp. upward) triangles indicate the lower (resp. upper) bound for the optimal policy computed according to Eq. (4) (resp. Eq. (5)). The lower bound is strict and assumes an omniscient agent. The upper bound corresponds to an exhaustive search following an outward spiral, except in 1D where an “end-to-end” trajectory is better (unless the domain is very small). The (thin) shaded area between infotaxis dots show 95 % confidence intervals.

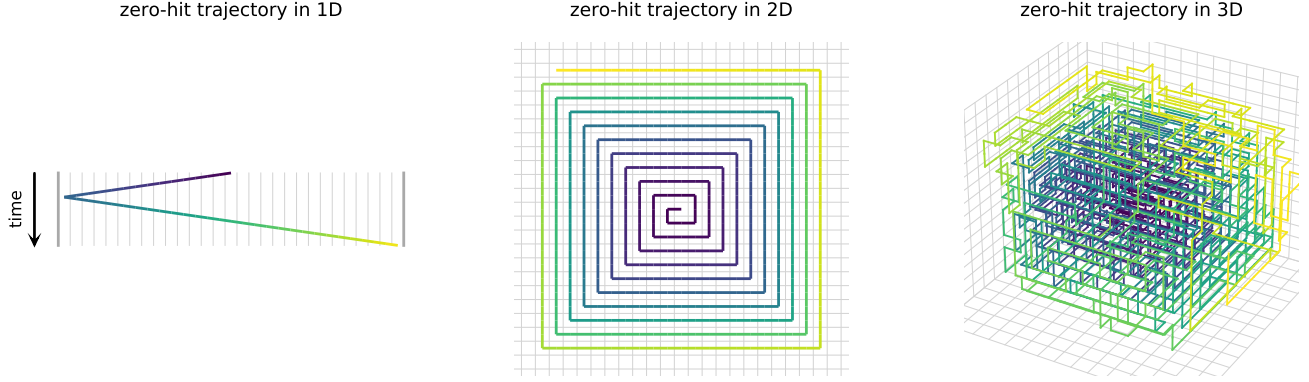


FIG. 13. Infotactic trajectories in the absence of cues (succession of zero hits in the limit $\mathcal{I} \rightarrow 0$) in 1D, 2D and 3D (columns). Time is color-coded from blue (start) to yellow (end). The grid is shown in grey.

many independent processes, by application of the central limit theorem in the log domain). They are often encountered in lifetime analysis when termination results from many small random multiplicative effects. Here termination (finding the source) is “caused” by the entire sequence of (policy-controlled) actions and (random) observations. Even though these successive events are correlated, their interdependence over long searches is weak enough in higher dimension to yield the lognormal signature.

To summarize, we computed the statistics of infotactic searches in 1D, 2D, 3D and 4D, for a wide range of dimensionless problem sizes $\mathcal{L} = \lambda/\Delta x$ and cue emission intensities $\mathcal{I} = R\Delta t$. Our data shows that infotaxis is *reliable* (the probability of failure is less than 10^{-3}), *efficient* (the mean search time scales as expected for the optimal policy), and *safe* (the tail of the distribution of search times decays faster than any power law, though subexponentially).

D. N-step infotaxis

Infotaxis is based on a one-step anticipation of possible outcomes of each action. Would infotaxis perform better if it anticipated two actions? three actions? N actions? In this section, we introduce the generalization of 1-step infotaxis to N-step infotaxis and report on its performance.

Let us first consider 2-step infotaxis, which consists in choosing the action that maximizes the expected gain of information after executing two actions. Formally, this reads

$$\pi^{\text{2-step infotaxis}}(s) = \arg \max_a \left\{ G(s, a) + \gamma \sum_{s'} \Pr(s'|s, a) \max_{a'} G(s', a') \right\} \quad (48)$$

where γ is a discount factor which we will discuss later on, and which controls the weight given to the gain expected from second action compared to that from the first action.

The expression given by Eq. (48) is better understood from Fig. 15, which illustrates how it is calculated. First, we expand the tree from belief state s (top node) and calculate all possible belief states s'' (bottom nodes) that can be reached after executing any combination of two actions a and a' . Each of these belief states has an associated entropy $H(s'')$. Then, we transfer this information back to the top node through successive reduction operations as follows (this procedure is sometimes called “backup” in tree-search planning and reinforcement learning) :

1. for each node s'' we calculate its entropy $H(s'')$;
2. for each node a' we can calculate the expected gain $G(s', a') = H(s') - H(s'|a')$ where $H(s'|a') = \sum_{s''} \Pr(s''|s', a') H(s'')$ (we simply applied Eqs. (40) and (41) to s' and a');
3. for each node s' we choose the infotactic action that maximizes $G(s'|a')$, that is, we associate each node s' to $\max_{a'} G(s'|a')$;
4. for each node a we can calculate $G(s, a)$ (the gain expected from action a) as well as $\sum_{s'} [\Pr(s'|s, a) \max_{a'} G(s'|a')]$ (the maximum gain expected from action a'), and we then associate each node a to the expected discounted cumulated gain $G(s, a) + \gamma \sum_{s'} [\Pr(s'|s, a) \max_{a'} G(s'|a')]$;
5. minimizing this last expression over possible actions a takes us back to the starting node s and yields Eq. (48).

The generalization to N_{steps} steps is straightforward from Fig. 15.

We now come back to the introduction of a discount factor, with $0 \leq \gamma \leq 1$. Discounting with factor γ means

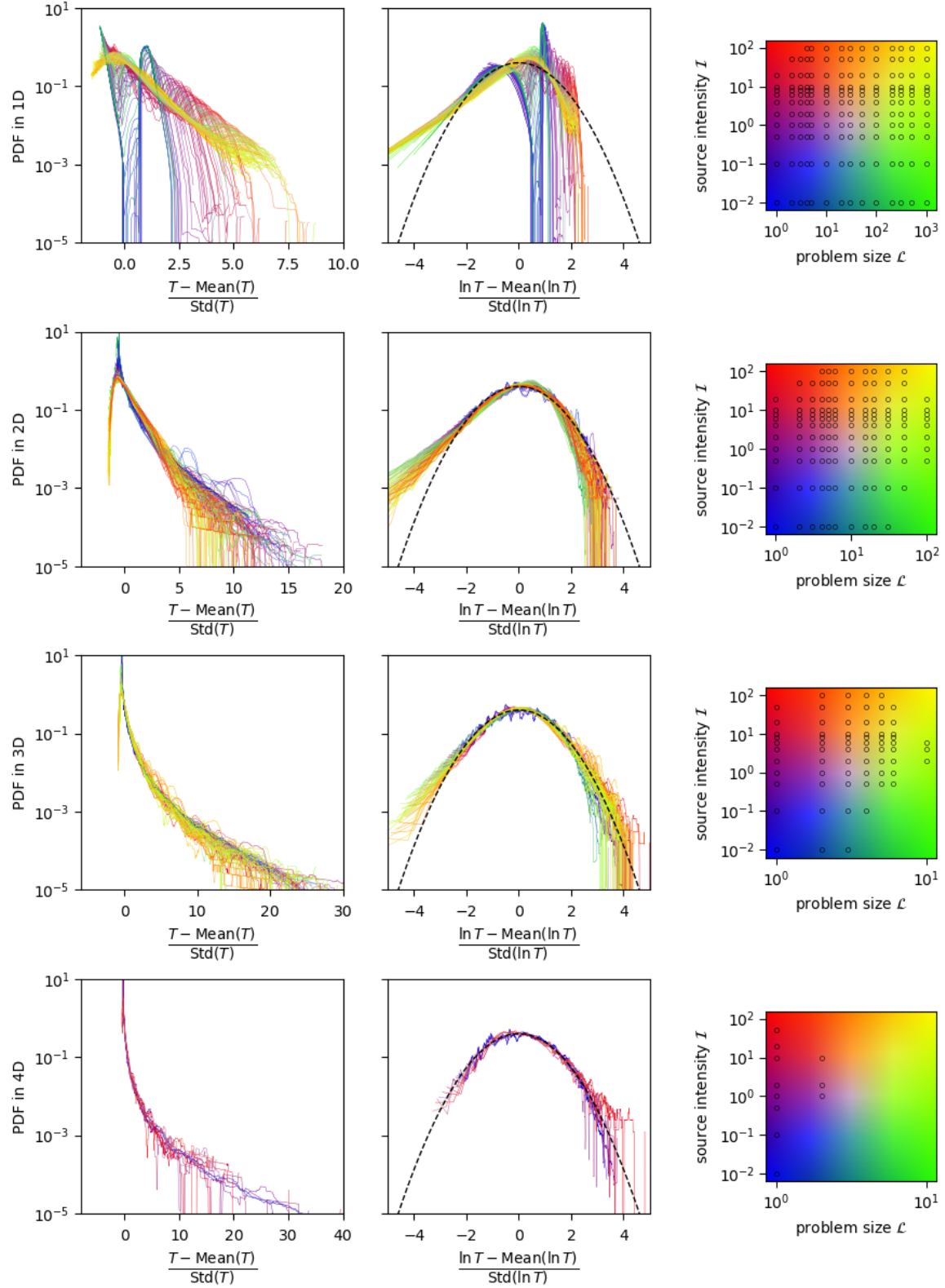


FIG. 14. Distributions of arrival times with infotaxis for source tracking in 1D, 2D, 3D and 4D (rows) for a wide range of problem sizes $\mathcal{L} = \lambda/\Delta x$ and source intensities $\mathcal{I} = R\Delta t$ (color-coded according to the map on the right). The same data is plotted in both columns using different scales to evidence the distribution features. In the left column, exponential decay would appear as linear. In the right column, a standardized lognormal distribution would appear as a parabola (dashed curve), which corresponds to a standard Gaussian in the log-lin space.

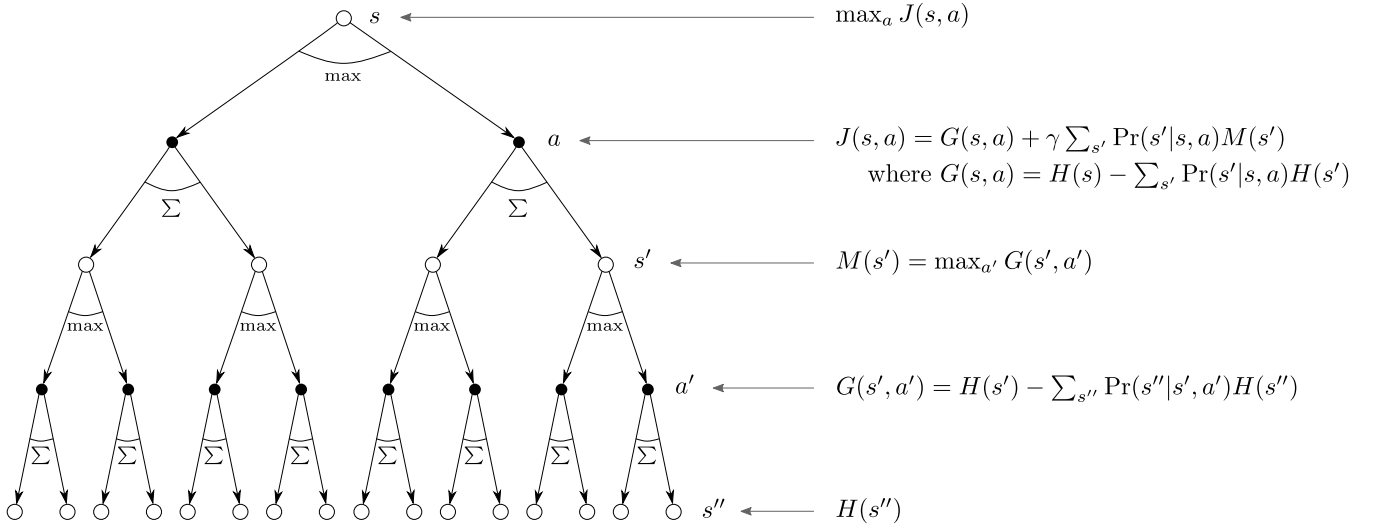


FIG. 15. Backup diagram for 2-step infotaxis.

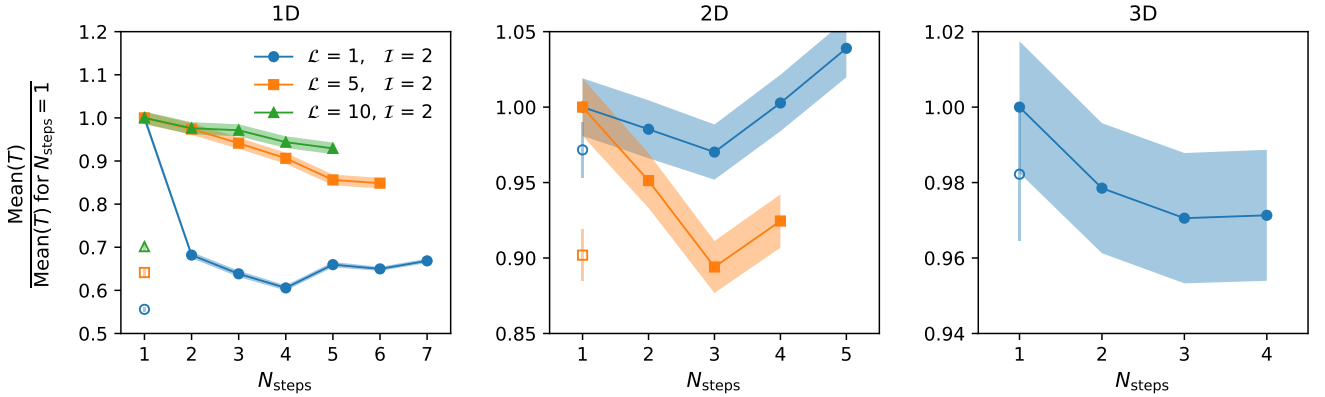


FIG. 16. Performance of N -step infotaxis in 1D, 2D and 3D (columns): mean number of steps to find the source as a function of the number of anticipated steps N_{steps} , normalized by its value for 1-step infotaxis (filled symbols). The shaded areas represent 95% confidence intervals. The discount factor is $\gamma = 0.999$. For comparison, we also show the performance of our “space-aware infotaxis” (SAI-1) with open symbols (cf. Section IV).

that an information gain received at the i -th step is worth only γ^{i-1} times what it would be worth at the first step, and translates the idea that gaining an amount now is better than gaining the same amount later. If $\gamma = 0$, all later gains are entirely discounted and one recovers (1-step) infotaxis. If $\gamma = 1$, all later gains have the same weight as the first one. This is not desirable, because this means, for example, that in a situation where the source can be surely found in either 1 or 3 steps, 3-step infotaxis would consider both options equal. In our numerical experiments we will use $\gamma = 0.999$, which alleviates the above-mentioned issue without discarding information from the deepest layers of the tree.

From a computational point of view, it is clear from Fig. 15 that the cost of N -step infotaxis is exponential in N_{steps} , it is therefore of very limited practical interest. Yet it is fundamentally interesting to determine whether a significant increase of computational power leads to

valuable improvements of infotaxis.

The performance of N -steps infotaxis as a function of the number of anticipated steps is reported in Fig. 16 for searches in 1D, 2D and 3D, and for a couple different problem sizes \mathcal{L} (we set $\mathcal{I} = 2$). Results are quite variable depending on the case considered. In 1D, improvements are significant for the smallest domain (up to a -40 % reduction in the mean search time for $\mathcal{L} = 1$) while more modest for larger domains (up to -15 and -7 % for $\mathcal{L} = 5$ and 10, respectively, though a plateau is not reached yet at $N_{\text{steps}} = 6$ and 5, respectively). In 2D, the search time is reduced by up to -3 % for the smallest domain ($\mathcal{L} = 1$), and by up to -11 % for a larger one ($\mathcal{L} = 5$). On the other hand, the 2D case with $\mathcal{L} = 1$ also shows an example where N -step infotaxis ($N_{\text{steps}} = 5$) performs worse than infotaxis. In 3D, improvements plateau at -3 %, though we tested only the smallest domain size.

Overall, the search duration first decreases as N_{steps}

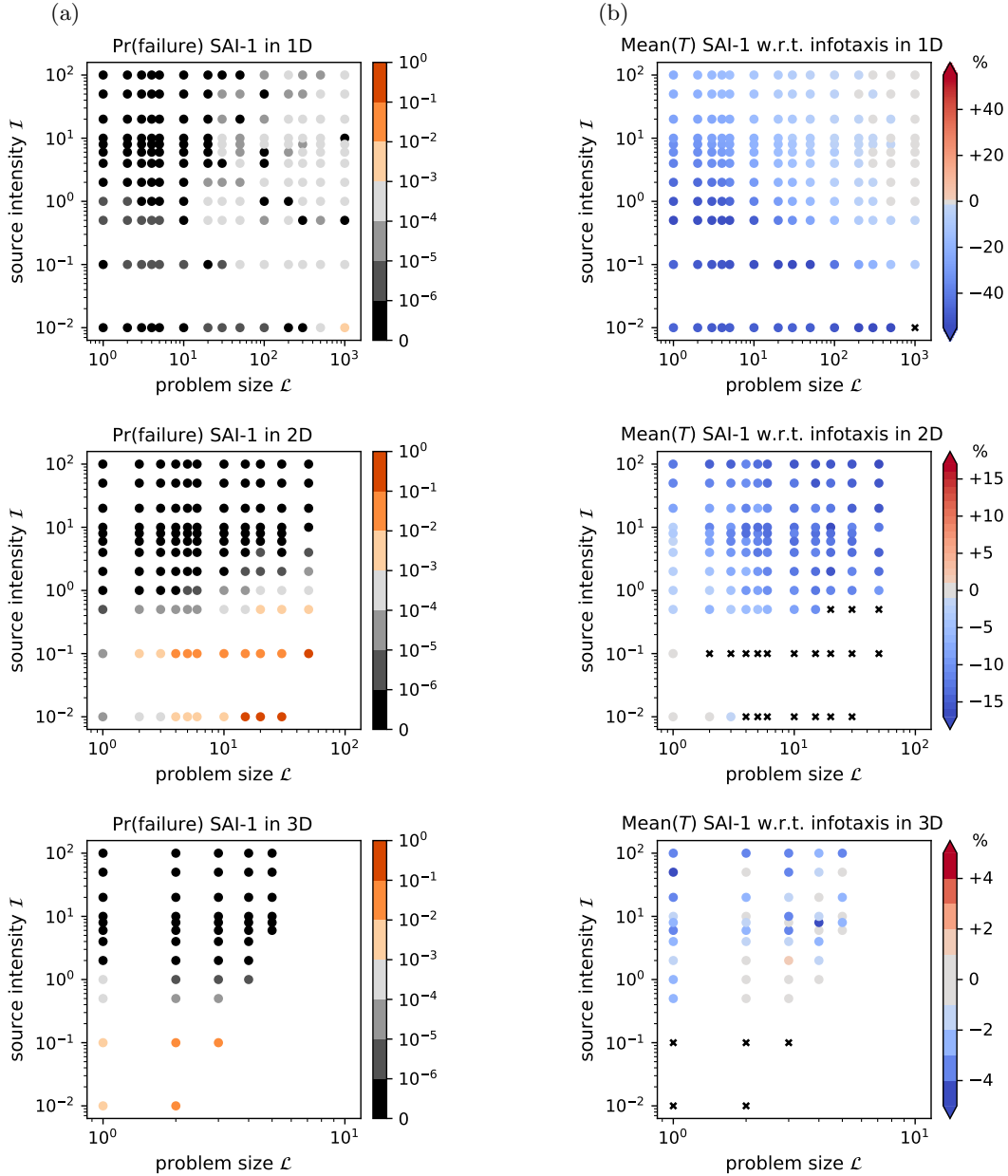


FIG. 17. Performance of Manhattan space-aware infotaxis (SAI-1) for source tracking in 1D, 2D, and 3D (rows), for a wide range of physical parameters $\mathcal{L} = \lambda/\Delta x$ and $\mathcal{T} = R\Delta t$: (a) probability of never finding the source and (b) relative difference in the mean number of steps to find the source compared to infotaxis (-10 % means that SAI finds the source in 10 % less time than infotaxis). In (b), the black crosses depict cases where $\text{Pr}(\text{failure}) > 10^{-3}$.

increases, and then either reaches a plateau or increases again as N_{steps} is increased further. This non-monotonic behaviour is another evidence of the absence of a linear correlation between entropy and remaining time to find the source. Importantly this minimum (or this plateau) does not generally correspond to the optimal performance: it is clear in 1D that our own heuristic, “space-aware infotaxis” (depicted by open symbols, and which will be presented in the next section) performs significantly better.

IV. BEATING INFOTAXIS: SPACE-AWARE INFOTAXIS

Infotaxis is inherently risk-averse, which explains why it is so reliable. But this behavior is not optimal: it is indeed known that shifting infotaxis toward more exploitation using a tunable parameter can reduce search duration [19, 20]. This is however not satisfying, since the optimal value of this parameter is not universal and requires manual tuning. Here we will present the first parameter-free policy that achieves better performance

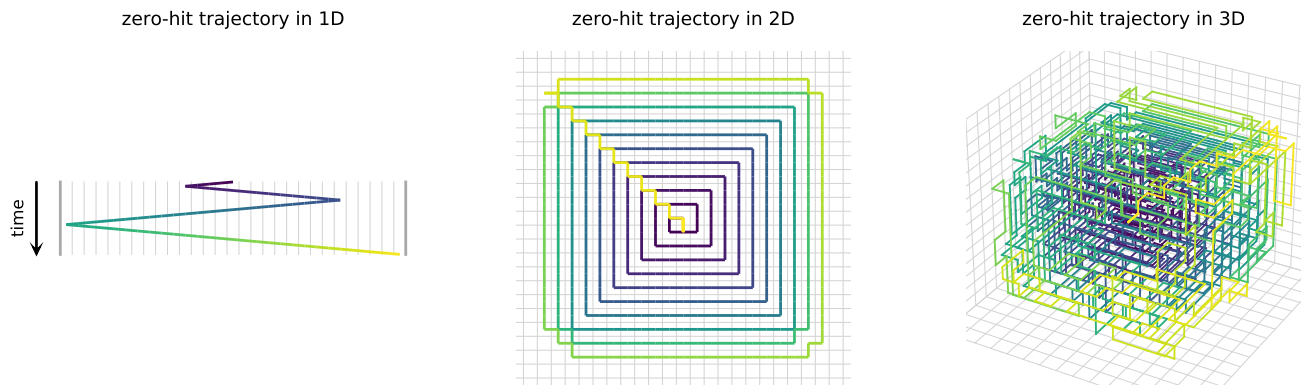


FIG. 18. Trajectories generated by space-aware infotaxis (SAI-1) in the absence of cues (succession of zero hits in the limit $\mathcal{I} \rightarrow 0$) in 1D, 2D and 3D (columns). Time is color-coded from blue (start) to yellow (end). The grid is shown in grey. To be compared to Fig. 13 for infotaxis.

than infotaxis.

Entropy is a quantity which does not contain any spatial information about the source possible location. To make infotaxis more exploitative, we will build a policy based on entropy H , which measures uncertainty, and on a spatial metric, denoted D , which quantifies the distance to the source.

The quantity we want to minimize should naturally balance H and D and be related to the time remaining to find the source. We chose the following expression:

$$J(s) = \log_2 \left(D(s) + 2^{H(s)-1} - \frac{1}{2} \right) \quad (49)$$

where the $H(s)$, the entropy of belief state s , has been defined in Eq. (39) and where $D(s)$ is the mean Manhattan distance between the agent and the source:

$$D(s) = \sum_{\mathbf{x}} p(\mathbf{x}) \|\mathbf{x} - \mathbf{x}^a\|_1. \quad (50)$$

This seemingly *ad hoc* expression of J has been constructed from the following considerations.

Consider a distribution $p(\mathbf{x})$ with entropy H . Assuming $p(\mathbf{x})$ were uniform, this corresponds to an effective number of cells $N_{\text{eff}} = 2^H$. The expected time to find a uniformly distributed source by visiting exhaustively N_{eff} cells is

$$\mathbb{E}[T] = \sum_{i=0}^{N_{\text{eff}}-1} \frac{i}{N_{\text{eff}}} = \frac{N_{\text{eff}} - 1}{2} = 2^{H-1} - \frac{1}{2}. \quad (51)$$

This expression does not take into account any spatial constraint and is derived assuming the agent can jump from cell to cell for a unit cost. On the other hand, if the source location is known, the minimal time needed to reach a source located at a distance D is D . Assuming the effects of distance and of uncertainty combine linearly, this gives the expression $D + 2^{H-1} - \frac{1}{2}$ as an estimate of the number of time steps remaining to find the source.

An additional consideration is the mathematical properties that we would like J to satisfy. For any (finite-horizon) belief-MDP with a cost to minimize, the optimal value function $v^*(s)$ of a belief state s , defined by Eq. (2), is necessarily a concave function of that belief state [34, 35]. Since J is designed to be an approximation of the optimal value function v^* , we applied a logarithm function to ensure that J is a concave function of $p(\mathbf{x})$. The particular choice of the logarithm is motivated by the fact that infotaxis is recovered if one enforces $D = 0$ (note that the entropy H is indeed a concave function of $p(\mathbf{x})$). It is very possible that another concave function would be a better choice, however the cost of the required simulations prevents us from assessing whether it is the case.

We now introduce “space-aware infotaxis” (SAI), the policy that minimizes the expected J at the next step. It reads

$$\pi^{\text{SAI}}(s) = \underset{a}{\operatorname{argmin}} J(s|a) \quad (52)$$

where $J(s|a)$ is the expected J upon executing action a in belief state s , which is given by

$$J(s|a) = \sum_{s'} \Pr(s'|s, a) J(s') \quad (53)$$

where the sum is taken over all successor belief states s' . Note that SAI looks one step ahead into possible futures, the same way infotaxis does, therefore its computational cost is essentially the same as infotaxis (the only extra computation required is that of D). As was the case with infotaxis, if $J(s)$ was linearly related to the expected remaining time $v^*(s)$ to find the source from s , this policy would be optimal.

The performance of SAI is plotted in Fig. 17 as a function of the dimensionless parameters of problem: the problem size \mathcal{L} and the source intensity \mathcal{I} (as defined by Eq. (15)). Video examples of its behavior are provided in Supplemental Material. We show the probability of

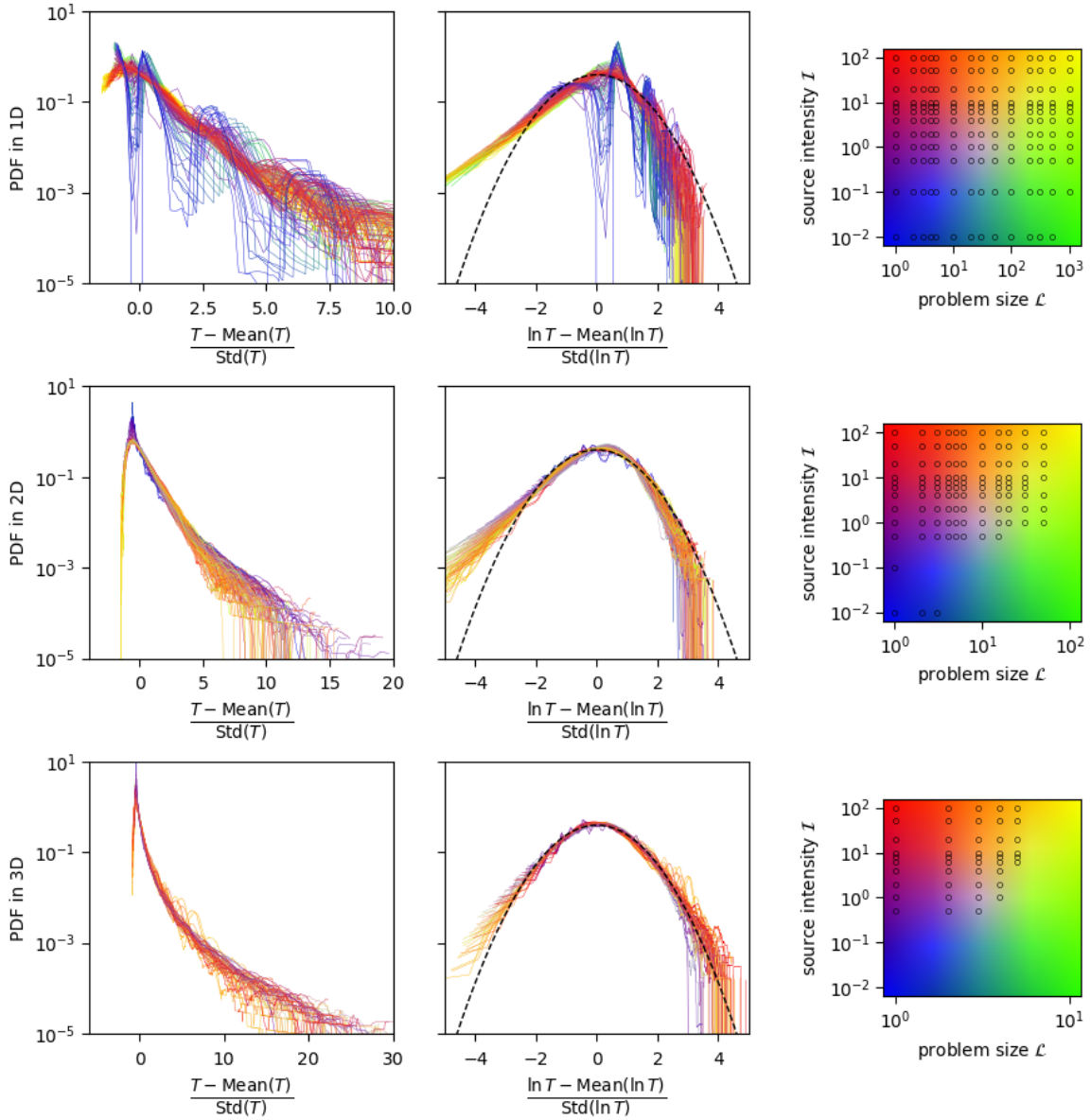


FIG. 19. Distributions of arrival times with Manhattan space-aware infotaxis (SAI-1) for source tracking in 1D, 2D and 3D (rows) for a wide range of problem sizes $\mathcal{L} = \lambda/\Delta x$ and source intensities $\mathcal{I} = R\Delta t$ (color-coded according to the map on the right). The same data is plotted in both columns using different scales to evidence the distribution features. The dashed line (right column) shows a standardized log-normal distribution. To be compared to Fig. 14 for infotaxis.

failure and the relative difference in the mean number of steps between SAI and infotaxis, defined such that a negative value signifies an improvement: for example a relative difference of -10 % means that SAI finds the source in 10 % less time than infotaxis, on average.

In 1D, SAI never fails and beats infotaxis everywhere by roughly 20 to 50 % in the lower left quadrant of the $(\mathcal{L}, \mathcal{I})$ parameter space, while improvements are more modest in the upper right quadrant. This impressive gain is due to the markedly different behavior of SAI in the absence of hits: while infotaxis tends to go to one end of the domain before turning back and going to the

other end, SAI goes back and forth, exploring the domain further each time, as depicted in Fig. 18. This behavior illustrates the more exploitative nature of SAI compared to infotaxis.

In 2D, SAI works only in the presence of cues ($\mathcal{I} \gtrsim 1$) but is able to reduce the time to find the source by roughly 5 to 15 %. In 3D, again SAI works only provided that the source intensity is not too small, and overall performs slightly better than infotaxis (roughly 2-3 % improvement overall). We did not evaluate SAI in 4D due to the high computational cost and to the error bar on infotaxis data which prevents meaningful comparisons.

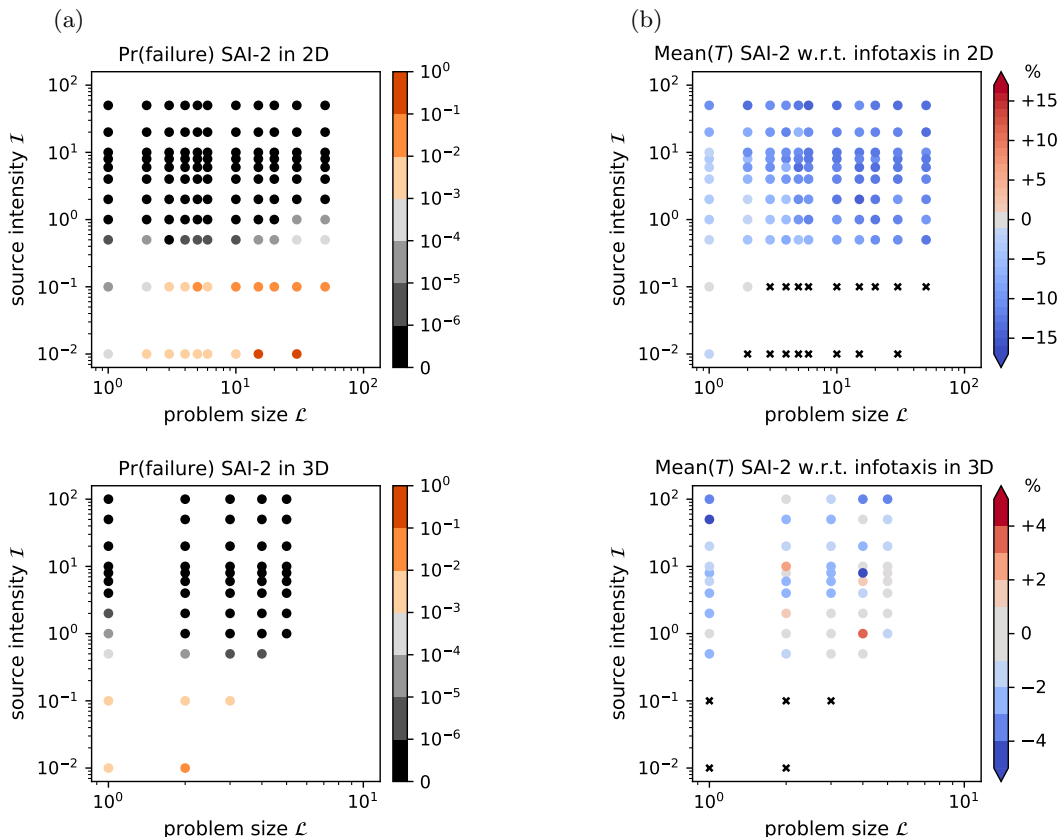


FIG. 20. Performance of Euclidean space-aware infotaxis (SAI-2) for source tracking in 2D and 3D (rows), for a wide range of physical parameters $\mathcal{L} = \lambda/\Delta x$ and $\mathcal{I} = R\Delta t$: (a) probability of never finding the source and (b) relative difference in the mean number of steps to find the source compared to infotaxis (-10 % means that SAI finds the source in 10 % less time than infotaxis). In (b), the black crosses depict cases where $\text{Pr}(\text{failure}) > 10^{-3}$. In 1D, Manhattan and Euclidean norms are equivalent.

The fact that SAI is not reliable for small source intensities is not an important issue, since in this case the search is essentially performed without cues, therefore one could simply use the exhaustive spiral search (which is what infotaxis reduces to in this limit). The lack of reliability of SAI in this case is due to the fact the SAI agent starts with a spiralling trajectory, but after a long period without hits, comes back to the center of the domain and remains trapped there, as illustrated in Fig. 18.

Importantly, if the source location is known, SAI will direct the agent toward it (in an optimal manner). In contrast, an infotactic agent will be lost in this situation (the entropy being zero, it can not be reduced any further). This explains why SAI is reliable for the high source intensities where infotaxis was shown to fail (cf. Fig. 10a).

The distributions of arrival times generated by SAI and by infotaxis exhibit the same features. In particular, the standard deviation is of the same order of the mean: for SAI we have $\text{Std}(T)/\text{Mean}(T) \in [0.6, 1.3]$ in 1D, $[0.7, 1.6]$ in 2D, and $[1.0, 2.3]$ in 3D; these values are comparable to those obtained with infotaxis. The standardized distributions of arrival times exhibit tails that are well described

by log-normal distributions akin to those obtained with infotaxis, as shown in Fig. 19. The only significant differences are the oscillations in the distribution of the 1D arrival times, particularly visible for small domains: they are the signature of the back-and-forth trajectories of SAI in 1D.

While the choice of the Manhattan norm in the definition of D (Eq. (50)) is the most intuitive, the Euclidean norm is also a natural candidate since it determines the occurrence of hits. In more than 1D, this choice may matter. Therefore we evaluated the performance of an alternative version of SAI, SAI-2, that uses the mean Euclidean distance between the agent and the source as the definition for D :

$$D(s) = \sum_{\mathbf{x}} p(\mathbf{x}) \|\mathbf{x} - \mathbf{x}^a\|_2. \quad (54)$$

The results, presented in Fig. 20, show that SAI-2 performs well, although marginally worse than SAI-1 (the version based on the Manhattan norm).

Finally, we add that various variants of infotaxis have been previously published, claiming to perform better, for example replacing the entropy gain by the Bhattacharyya distance [28] or maximizing the uncertainty

on the next observation [24]. We tested those, and found this is not the case in our setup.

V. TOWARD THE OPTIMAL POLICY: DEEP REINFORCEMENT LEARNING

In this section, we show how deep reinforcement learning can be applied to the source-tracking problem. Our goal here is not to perform of complete study of the capabilities of reinforcement learning to solve the source-tracking problem, which could easily be an entire study on its own. Instead, we wish to report on our (successful) attempt to solve, for the first time, the source-tracking POMDP using deep reinforcement learning in order to approach at best the optimal policy, as well as to provide a point of comparison to heuristic policies such as infotaxis.

A. Reinforcement learning algorithm

In short, our reinforcement learning algorithm is based on DQN [36] (an extension of traditional Q-learning to deep neural networks), but is adapted here to take advantage of the fact that we have access to the model that determines the transitions between a belief state and all its successors. A detailed introduction to this algorithm is presented in the remainder of this section.

We first recall that (truly) solving the source-tracking problem means finding the optimal policy, as explained in Section II B. For that, one needs to compute the optimal value function $v^*(s)$, which is the function that satisfies Eq. (2) for all belief states s . If belief states could be tabulated, v^* could be obtained by classical dynamic programming using a value iteration algorithm [15, 31]. Since there are infinitely many belief states, we must resort to an approximate solution method.

We approximate $v^*(s)$ by a parameterized functional form $\hat{v}(s; \mathbf{w})$ with weight vector \mathbf{w} . In practice here, \hat{v} is the function computed by a multi-layer artificial neural network, and \mathbf{w} is the vector containing all “synaptic” weights. The optimal Bellman equation for the approximate value function is

$$\hat{v}(s; \mathbf{w}^*) = \min_a \sum_{s'} \Pr(s'|s, a) [1 + \hat{v}(s'; \mathbf{w}^*)] \quad \forall s \neq s^\Omega \quad (55)$$

with $\hat{v}(s^\Omega; \mathbf{w}^*) = 0$, and the problem becomes that of finding the weights \mathbf{w}^* that allow Eq. (55) to be satisfied “at best”, that is, the weights that minimize the residual error. This residual error, called the optimal Bellman error, reads

$$L(\mathbf{w}) = \mathbb{E}_s \left[\min_a \sum_{s'} \Pr(s'|s, a) [1 + \hat{v}(s'; \mathbf{w})] - \hat{v}(s; \mathbf{w}) \right]^2 \quad (56)$$

where the expectation is taken over belief states s visited when following the policy $\hat{\pi}$ derived from \hat{v} and defined by

$$\hat{\pi}(s; \mathbf{w}) = \arg \min_a \sum_{s'} \Pr(s'|s, a) [1 + \hat{v}(s'; \mathbf{w})]. \quad (57)$$

The functional $L(\mathbf{w})$ is, in the language of deep neural networks, known as the “loss function”, and “training” the network then refers to the iterative update (through stochastic gradient descent) of the weights \mathbf{w} so as to minimize this loss function (here defined in a least square sense, but other norms may be more appropriate depending on the problem).

It is well known that basic training algorithms (such as Q-learning) are unstable or even diverge when nonlinear function approximators (such as deep neural networks) are used to represent value functions. This major issue was overcome with DQN [36], a reinforcement learning algorithm which assembled various stabilization techniques (experience replay, delayed target network) to facilitate (though not guarantee) convergence, and which capabilities were demonstrated by achieving super-human performance on classic Atari video games such as Pong, Breakout and Space Invaders (to name a few).

Most reinforcement learning algorithms, including Q-learning and DQN, are model-free, and hence rely on the so-called action-value function (also known as the “Q function”). The source-tracking problem is, however, model-based, because the probability of transitioning from a belief state s to a successor belief state s' is known exactly for all possible successor belief states. This allows us to work directly with the value function \hat{v} , and to perform a full backup (that is, to compute the sum over s' in Eqs. (55–57)) rather than a sample backup (based on a single successor belief state randomly sampled).

Our reinforcement learning algorithm is therefore identical to DQN [36], except that the network is trained to approximate the value function rather than the action-value function, and uses full backups rather than sample ones. Further technical information (neural network architecture, hyperparameters, etc.) is provided in Appendix B 2. Our reinforcement learning algorithm is freely available as part of our open-source code [the code will be released upon acceptance].

B. Performance of (near) optimal policies

Training was interspersed with periodic evaluations of the current policy $\hat{\pi}$ in order to monitor its progress. Some examples of the evolution of the performance during training are shown in Fig. 21. After a transient, the performance reaches a plateau, which signifies that training is complete (the weights of neural network have converged). This trained neural network defines our learned policy. For each case, we increased the size (width and depth) of the neural network until the performance of

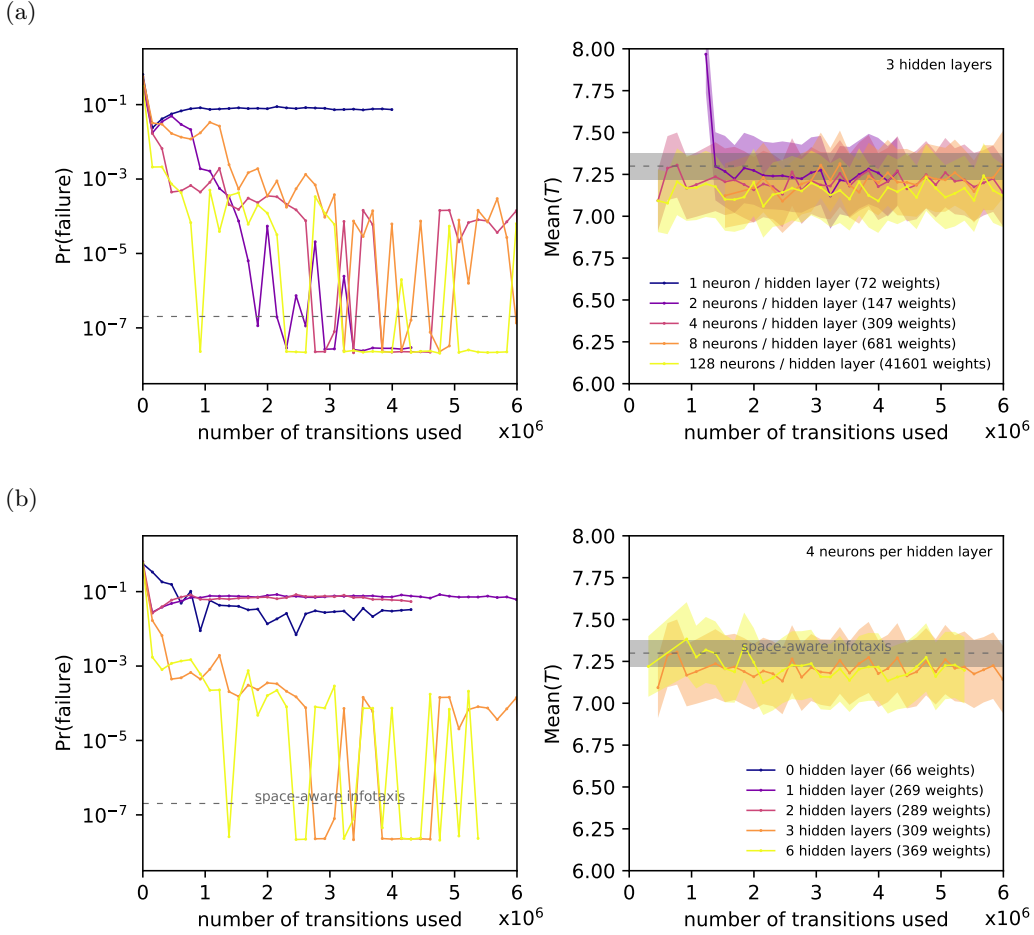


FIG. 21. Evolution of performance during training for increasing network sizes: (a) increasing widths and (b) increasing depths. Performance is measured by $\text{Pr}(\text{failure})$, the probability of never finding the source (left), and by $\text{Mean}(T)$, the mean number of steps to reach it (right, shown only provided that $\text{Pr}(\text{failure}) < 10^{-3}$). Performance of the trained network is very reproducible over various trials, and converges to a well-defined value as the network size is increased: this defines our optimal (or near optimal) performance. Here the training was performed for a 1D search with $\mathcal{L} = 2$ and $\mathcal{I} = 2$ (grid size is $N = 33$, neural network input size is 65). The dashed lines show the performance of space-aware infotaxis. Shaded areas show 95 % confidence intervals.

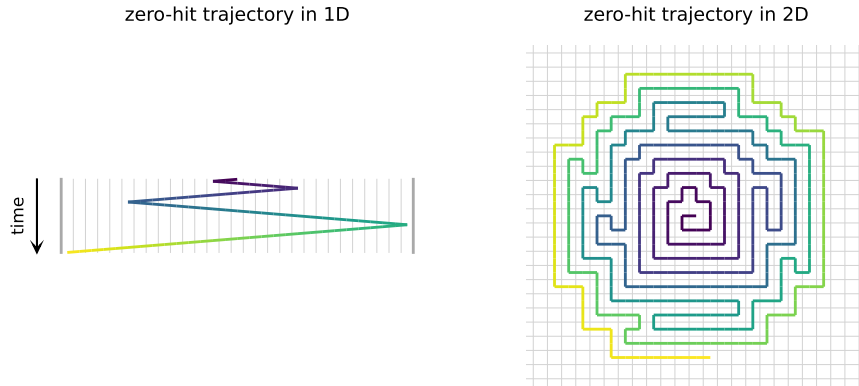
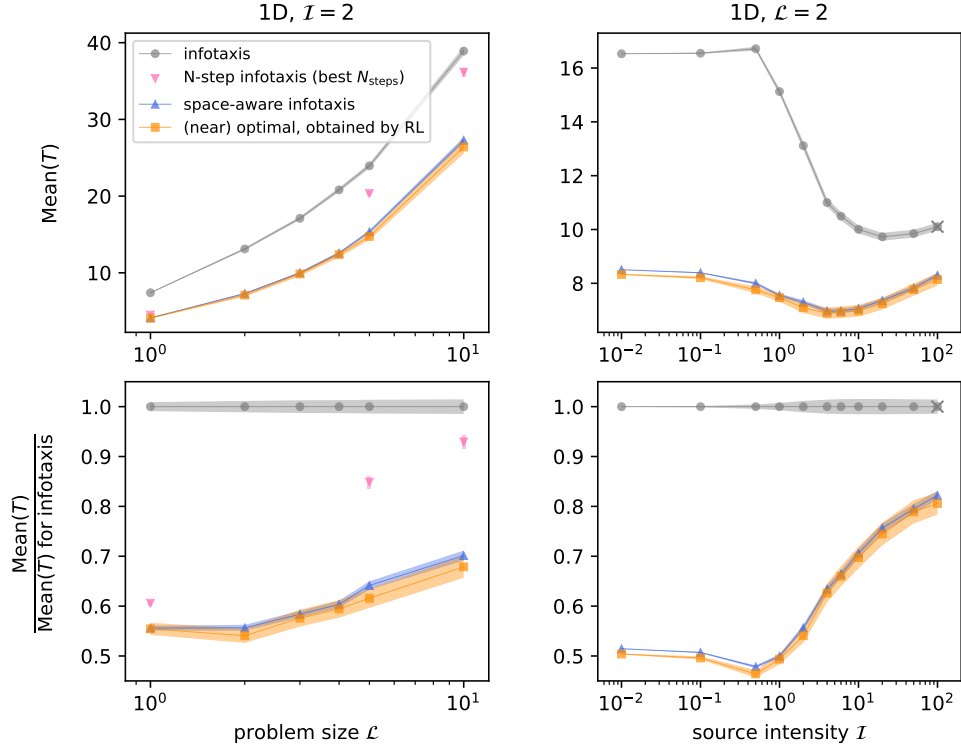


FIG. 22. Optimal (or near optimal) trajectories in the absence of cues (succession of zero hits in the limit $\mathcal{I} \rightarrow 0$) in 1D and 2D, obtained by deep reinforcement learning. Time is color-coded from blue (start) to yellow (end). The grid is shown in grey. To be compared to Fig. 13 for infotaxis and to Fig. 18 for space-aware infotaxis.

(a)



(b)

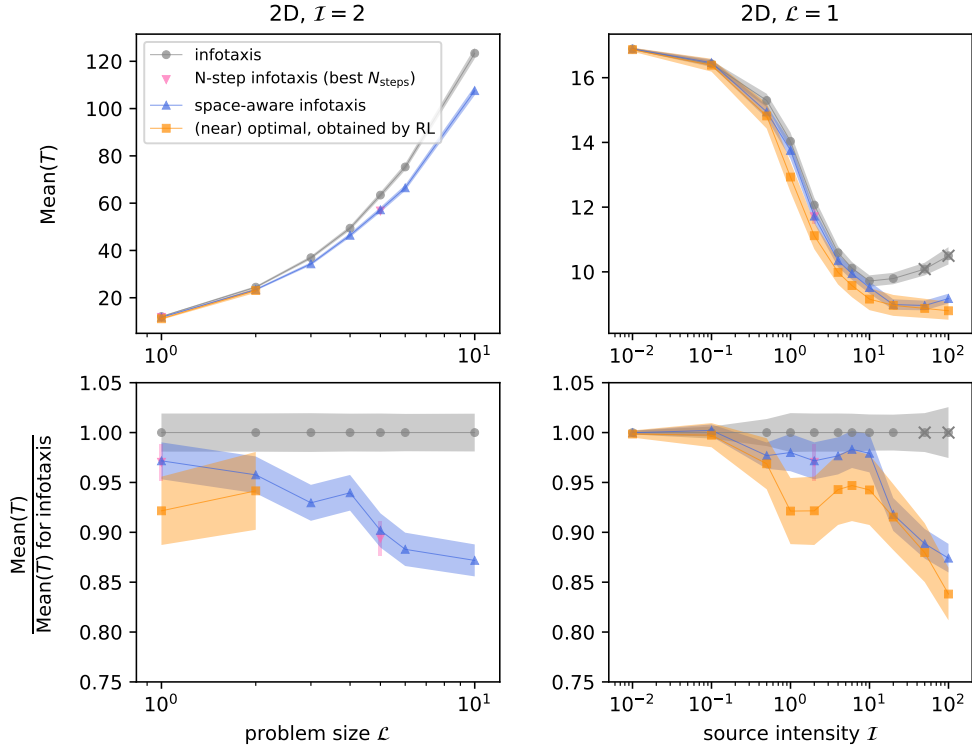


FIG. 23. Performance of (near) optimal policies obtained by deep reinforcement learning (RL) in (a) 1D and (b) 2D: mean number of steps to find the source as a function of the problem size $\mathcal{L} = \lambda/\Delta x$ (left) and the source intensity $\mathcal{I} = R\Delta t$ (right). All RL policies have $\text{Pr}(\text{failure}) < 10^{-6}$. For comparison we also show the performance of infotaxis, space-aware infotaxis (SAI-1) and N-step infotaxis (when available). Crosses indicate that $\text{Pr}(\text{failure}) > 10^{-3}$. Shaded areas show 95 % confidence intervals.

the learned policy converges, as illustrated for a case in Fig. 21: this is a good indication (though not a proof) that the learned policy is optimal or very close to optimal. Due to the high cost of training and of ensuring that the learned policies were as close as possible to optimal, we trained policies only for small 1D and 2D domains (problem size $\mathcal{L} = O(1)$). Importantly, neural networks were trained from scratch (random initial weights) and all the results we present are very reproducible (e.g., for different random initializations) (see Appendix B 2). Several videos that illustrate the behavior of these (near) optimal policies computed with reinforcement learning are available in Supplemental Material.

In the limit of a vanishing source intensity ($\mathcal{I} \rightarrow 0$), the search is performed without cues and the trajectories are deterministic (succession of zero hits). The (near) optimal trajectories are shown in Fig. 22. In 1D, the trajectory is qualitatively similar (but not identical) to the one generated by space-aware infotaxis (cf. Fig. 18) with a ‘back and forth’ motion extending further each time. In 2D, the trajectory is essentially an exhaustive spiral, as we obtained with infotaxis (cf. Fig. 13) and space-aware infotaxis (although the latter was interrupted, see Fig. 18). Its geometry is however different, since it seems to approximate a continuous Archimedean spiral defined with a Euclidean norm, rather than one defined with Chebyshev norm (as was the case with infotaxis and space-aware infotaxis). Repeated trainings produced slightly different trajectories, though all looked very similar to the one shown in Fig. 22. In continuous space, the Euclidean Archimedean spiral can be proven to be the optimal path for $\mathcal{I} \rightarrow 0$ using the fact that p_0 (the initial source probability distribution) is a monotonically decreasing function of the initial distance to the agent. Infotaxis has been shown to follow such a spiral in continuous space [22], hence the differences we observe here between (space-aware) infotaxis and the reinforcement learning policy are only due to our discrete setting.

The (near) optimal performance of learned policies is reported in Fig. 23 for searches in 1D and 2D with varying source intensities \mathcal{I} , and, to some extent, varying problem sizes \mathcal{L} (these dimensionless parameters are defined by Eq. (15)). Importantly all these learned policies have $\text{Pr}(\text{failure}) < 10^{-6}$. For comparison we also show the performance of infotaxis, N-step infotaxis and space-aware infotaxis on the same figure. In 1D, the mean time to find the source can be reduced by roughly 20 to 50 % compared to infotaxis. In 2D, this reduction is roughly around 5-10 %, and up to 16 %.

The most surprising result is maybe the remarkable performance of space-aware infotaxis: for all cases considered here, the performance attained with our heuristic is very close to the (near) optimal one obtained by deep reinforcement learning. It will be very interesting to evaluate to which extent this result generalizes to larger domain sizes and to 3 dimensions, however the amount of computations required to ensure (near) optimality in 3D is beyond our resources.

VI. DISCUSSION AND CONCLUSION

In this paper we demonstrated that infotaxis is generally suboptimal and can be beaten by other heuristics or by reinforcement learning, in particular for searches in lower dimensional spaces (and so even if an anticipation over multiple steps rather than one step is allowed). Yet, it remains a strong contender because of its generality: indeed infotaxis performs well over a huge range of parameters without any tuning. More precisely, we have shown that (i) the probability of failing to find the source is negligible (infotaxis is *reliable*), (ii) the mean search time scales with physical parameters as one would expect for the optimal policy (infotaxis is *efficient*), and (iii) the tail of the distribution of search times decays faster than any power law, though subexponentially (infotaxis is not plagued by large fluctuations and hence is *safe*) for essentially all combinations of physical parameters and up to 4D. Finally, we have shown that infotaxis can be made more efficient if the uncertainty measure (entropy) is balanced by a distance measure. We called this parameter-free policy ‘space-aware infotaxis’. Overall, this new heuristic reduces the mean time to find the source by 10-50 % in 1D, 5-15 % in 2D, and 2-3 % in 3D.

To provide a firmer answer to the question of how good infotaxis is, one needs to compare it to the optimal policy. The nature and the size of the source-tracking problem do not allow the computation of exact solutions, however finding approximately optimal solutions is a task well-suited for reinforcement learning. Our learning algorithm is a model-based version of DQN [36] where the value function is approximated by a deep neural network. We used large neural networks in order to approach at best the optimal policy. For this reason, we trained policies only for small domain sizes in 1D and 2D. Our results demonstrate that policies superior to infotaxis can be learned from scratch purely from experience. We found that, for the cases considered, the mean time to find the source can be reduced by 20-50 % in 1D and 5-15 % in 2D compared to infotaxis. Almost identical improvements were obtained by our space-aware infotaxis in those cases. Overall, this strongly suggests that (i) while infotaxis is vastly suboptimal in 1D, the margin of improvement toward the optimal policy gets tighter as the dimensionality increases and (ii) space-aware infotaxis is probably a very good approximation of the optimal policy.

So, why does infotaxis work so well? A theoretical argument was proposed in ref. [5], where the authors show that given a probability distribution $p(\mathbf{x})$ with entropy H , the expected optimal search time satisfies $\mathbb{E}_{\pi^*}[T|p_0 = p(\mathbf{x})] \geq 2^{H-1}$, and conclude that reducing entropy is a necessary condition to an efficient search. This bound is, according to the authors, a lower bound because it assumes the agent can jump to any cell for a unit cost. This result, however, is derived assuming a frozen distribution $p(\mathbf{x})$ and therefore only holds in the absence of cues gathered along the search ($\mathcal{I} \rightarrow 0$). This is the same assumption we actually used to derive our up-

per bound in Eq. (5) based on an exhaustive search, and also for our estimate of the remaining time for space-aware infotaxis in Eq. (51). It can be easily verified, from our data but also from Fig. 2c in [5], that it is not a valid lower bound for a search with cues. Besides, based on this argument, one should seek to minimize the expectation of 2^{H-1} at the next step, rather than that of H (since these expressions are not linearly related, their expectations may rank actions differently). We actually tested this idea, and found that it does not perform as well as infotaxis.

We believe that the correct theoretical argument lies in the concavity of the optimal value function. This argument was provided in early artificial intelligence papers on POMDPs [16, 37], where the idea of entropy minimization was proposed for robotic navigation. We first need to remind the reader that solving the source-tracking problem is equivalent to computing its optimal value function v^* , defined for any belief state as the minimum expected number of remaining steps, starting from that belief state, over all possible policies. The optimal policy is then to choose the action that minimizes the expected optimal value at the next step. It can be mathematically proven that the optimal value function is a concave function of the belief state, in our case $p(\mathbf{x})$ [34, 35]. The concavity of the optimal value function implies that the lowest values correspond to belief states located at the corners of the belief space, where $p(\mathbf{x}) = \delta(\mathbf{x} - \mathbf{x}')$: these are also the belief states with the lowest entropy. It is therefore likely that minimizing the optimal value or minimizing the entropy yield the same action when uncertainty is high.

Quoting Kaelbling et al. [37] for an intuitive explanation: “The [concavity] of the optimal value function makes intuitive sense when we think about the value of belief states. States that are in the ‘middle’ of the belief space have high entropy – the agent is very uncertain about the real underlying state of the world. In such belief states, the agent cannot select actions very appropriately [...]. In low-entropy belief states, which are near the corners of the simplex, the agent can take actions more likely to be appropriate for the current state of the world [...]. This has some connection to the notion of ‘value of information’, where an agent can incur a cost to move it from a high-entropy to a low-entropy state; this is only worthwhile when the value of the information (the difference in value between the two states) exceeds the cost of gaining the information.”

As we have seen in this paper, beating infotaxis seems to be increasingly difficult as the dimensionality increases. While this could be inherent to the greater difficulty of finding good approximate solutions in higher dimensions, this result is well explained by the above argument: higher dimensionality implies larger uncertainty ($H \sim n \log N$, with n the dimension and N the linear domain size), meaning that optimal actions are those which help disambiguate the true source location (those which reduce entropy) for a larger fraction of the entire search.

Through this paper we illustrated three possible routes to improve on an existing heuristic solution: (i) tree search based on this heuristic (N-step infotaxis), (ii) knowledge-based approximation of the optimal value function (space-aware infotaxis), and (iii) deep reinforcement learning (that yielded near-optimal policies without any prior human knowledge). These approaches, adapted from those developed in artificial intelligence and related disciplines, were successfully applied to the source-tracking problem. There is no reason to believe they would not be successful at solving a broad range of decision-making problems constrained by physics, as routinely encountered in biophysics and robotics.

The source-tracking problem was inspired by olfactory searches performed by moths, which use pheromones to locate their mates [2, 3]. A similar navigation task is also faced by planktonic organisms such as copepods [4]. It is not plausible that these animals perform infotaxis as presented here [38]: infotaxis involves complex computations (due to the 1-step lookahead into possible futures) and relies on unrealistic assumptions (physical space representation, perfect memory, model knowledge). Developing heuristic approximations of infotaxis with much weaker requirements is possible [19], and it will be interesting to see whether such memory-based strategies can be discovered by minimal recurrent neural networks through reinforcement learning, as recently achieved for chemotaxis [39].

Besides, reinforcement learning has recently emerged as a powerful tool for finding nontrivial solutions to complex navigation problems in turbulent flows [40–44], and provides a complementary approach to physics-based heuristics [45]. While all these navigation problems are POMDPs, they have never been explicitly framed as such and hence never exploited existing mathematical results and algorithms developed for this class of problems. In addition, learned policies are most often memoryless, while it is clear that navigation strategies shaped by Darwinian evolution rely on memory, either in a physical (molecular) form for single cells (e.g., bacteria performing chemotaxis [46, 47]) or in an abstract one for higher organisms with cognitive capabilities (from the worm *C. elegans* to humans).

We believe that combining ideas from infotaxis (as a viable alternative to physical gradient climbing), Bayesian inference (for memory encoding) and POMDPs (which provide the mathematical framework) while leveraging the power of deep reinforcement learning is a promising route for uncovering search and navigation strategies used by living organisms and for adapting those to robotic applications. Through this paper, we made a first step in this direction by bringing together the relevant concepts and methods, and we hope to trigger further interest from all relevant communities on this highly interdisciplinary topic.

ACKNOWLEDGMENTS

This project has received funding from the European Research Council (ERC) under the European Union's Horizon 2020 research and innovation programme (grant agreement No 834238). Centre de Calcul Intensif d'Aix-Marseille is acknowledged for granting access to its high performance computing resources.

Appendix A: Derivation of the propagation-detection model in n dimensions

1. Model of propagation

We first derive the expression of the mean concentration of odor particles due to a point source. A source located at \mathbf{x}^s emits detectable particles at rate R with finite lifetime τ , which disperse in an isotropic medium characterized by an effective diffusivity D . The mean stationary concentration field $c(\mathbf{x}^a|\mathbf{x}^s)$ satisfies

$$D\nabla^2 c(\mathbf{x}^a|\mathbf{x}^s) - \frac{1}{\tau} c(\mathbf{x}^a|\mathbf{x}^s) + R\delta(\mathbf{x}^a - \mathbf{x}^s) = 0. \quad (\text{A1})$$

The solution is

$$c(\mathbf{x}^a|\mathbf{x}^s) = -\frac{R}{D}G(\mathbf{x}^a|\mathbf{x}^s) \quad (\text{A2})$$

where $G(\mathbf{x}^a|\mathbf{x}^s)$ is the Green's function of the Helmholtz operator $\nabla^2 + k^2$ with $k = i/\sqrt{D\tau}$. Explicitly, the solution reads, for any number of dimensions n ,

$$c(\mathbf{x}^a|\mathbf{x}^s) = \frac{R}{D} \frac{1}{(2\pi)^{n/2}} \left(\frac{1}{\lambda d}\right)^{n/2-1} K_{n/2-1}(d/\lambda) \quad (\text{A3})$$

where $d = \|\mathbf{x}^s - \mathbf{x}^a\|_2$, where $\lambda = \sqrt{D\tau}$ is a characteristic lengthscale for dispersion, and where K_ν is the modified Bessel function of the second kind of order ν .

In particular

$$n = 1 : \quad c(\mathbf{x}^a|\mathbf{x}^s) = \frac{R}{D} \frac{\lambda}{2} \exp(-d/\lambda), \quad (\text{A4a})$$

$$n = 2 : \quad c(\mathbf{x}^a|\mathbf{x}^s) = \frac{R}{D} \frac{1}{2\pi} K_0(d/\lambda), \quad (\text{A4b})$$

$$n = 3 : \quad c(\mathbf{x}^a|\mathbf{x}^s) = \frac{R}{D} \frac{1}{4\pi d} \exp(-d/\lambda). \quad (\text{A4c})$$

2. Model of detection

We now derive the mean number of odor particles detected by the agent using a simple model of chemoreception [48, 49] in the agent's neighborhood (far from the source) based on the assumption that the agent acts as a perfect sink for those particles.

Consider an agent modeled as an n -ball (ball of dimension n) with radius a in a medium with diffusion length-scale $\lambda \gg a$. Suppose that the agent's surface is fully

covered in receptors, and that every particle that reaches the surface is absorbed, such that the concentration on the ball surface is zero. Far from the agent, the concentration field is c_∞ . In a frame of reference center on the agent, and introducing ρ as the distance to the origin, the stationary concentration c in the near-field satisfies

$$\nabla^2 c = 0 \quad \text{with } \nabla^2 = \partial_\rho^2 + \frac{n-1}{\rho} \partial_\rho \quad (\text{A5})$$

with boundary conditions

$$c(\rho = a) = 0, \quad c(\rho \rightarrow \lambda) \rightarrow c_\infty. \quad (\text{A6})$$

Note that the introduction of the cut-off lengthscale λ in the second boundary condition is required to regularize the solution in 1D and 2D, which otherwise diverges.

The solution is

$$n = 1 : \quad c(\rho) = \frac{c_\infty}{\lambda - a} (\rho - a), \quad (\text{A7a})$$

$$n = 2 : \quad c(\rho) = \frac{c_\infty}{\ln(\lambda/a)} \ln(\rho/a), \quad (\text{A7b})$$

$$n = 3 : \quad c(\rho) = c_\infty \left[1 - \left(\frac{a}{\rho}\right) \right], \quad (\text{A7c})$$

$$n \geq 3 : \quad c(\rho) = c_\infty \left[1 - \left(\frac{a}{\rho}\right)^{n-2} \right]. \quad (\text{A7d})$$

The total flux toward the agent corresponds to the average number of particles which, due to their random motion, collide with its surface and are absorbed per unit time. It reads

$$J = D \left. \frac{dc}{d\rho} \right|_{\rho=a} S_n \quad (\text{A8})$$

where S_n is the surface area of the n -ball

$$S_n = \frac{2\pi^{n/2} a^{n-1}}{\Gamma(n/2)} \quad (\text{A9})$$

with Γ the gamma function. Explicitly this reads

$$n = 1 : \quad J = 2D \frac{c_\infty}{\lambda - a}, \quad (\text{A10a})$$

$$n = 2 : \quad J = 2\pi D \frac{c_\infty}{\ln(\lambda/a)}, \quad (\text{A10b})$$

$$n = 3 : \quad J = 4\pi a D c_\infty, \quad (\text{A10c})$$

$$n \geq 3 : \quad J = \frac{2\pi^{n/2} (n-2) a^{n-2}}{\Gamma(n/2)} D c_\infty. \quad (\text{A10d})$$

The expressions for the flux and for the mean field concentration can be matched by requiring that $c_\infty = c(\mathbf{x}^a|\mathbf{x}^s)$. The mean number of particles detected during a time Δt is $\mu = J\Delta t$, which yields the expressions given in Eq. (8).

```

pdf[i] ← 0 for all i // probability density function f(T) to be filled
Nepisodes ← 0
converged_stats ← False
while not converged_stats do
  Nepisodes ← Nepisodes + 1
  agent ← init_agent() // agent's position, initially at the center of the domain
  p_source ← init_p_source() // source probability distribution, initially drawn from set of priors
  t ← 0
  agent_stuck ← False
  p_not_found ← 1.0 // probability that the source has not been found yet
  episodic_pdf[i] ← 0 for all i // pdf of arrival times for this episode
  while p_not_found > ε_stop and not agent_stuck do
    t ← t + 1
    action ← policy(agent, p_source)
    agent ← move(agent, action)
    p_end ← p_source[agent] // probability that the source is in the agent's cell
    episodic_pdf[t] ← p_not_found * p_end
    p_not_found ← p_not_found * (1.0 - p_end)
    p_source ← Bayes_update_after_source_not_found(agent, p_source) // given by Eq. (12)
    hit ← draw_random_hit(agent, p_source) // according to Eq. (27)
    p_source ← Bayes_update_after_hit_received(agent, p_source, hit) // given by Eq. (13)
    agent_stuck ← is_agent_stuck()
  end while
  pdf[i] ← pdf[i] + episodic_pdf[i] for all i
  converged_stats ← are_stats_converged()
end while
pdf[i] ← pdf[i]/Nepisodes for all i // compute f(T) by averaging over episodic pdfs
return pdf

```

FIG. 24. Pseudo-code for efficient computation of probability density function $f(T)$ with our hybrid Bayesian/Monte-Carlo method. The norm of $f(T)$ is the probability of (ever) finding the source and is, in general, less than one.

Appendix B: Technical details on the code

Our code is entirely open-source and freely downloadable [the code will be released upon acceptance]. In this Appendix we provide some additional details on the algorithms we use.

1. Hybrid Bayesian/Monte-Carlo method for statistics computation

The pseudo-code for computing the distribution of arrival times $f(T)$ using the “hybrid Bayesian/Monte-Carlo” method is given in Fig. 24.

2. Deep reinforcement learning algorithm

a. Deep neural network

The approximate value function $\hat{v}(s; \mathbf{w})$ is a neural network with weights \mathbf{w} that takes the belief state $s = [\mathbf{x}^a, p(\mathbf{x})]$ in input and returns its value (a scalar).

a. *Preprocessing* The belief state, which contains both the agent’s position (an n -tuple) and the source probability distribution (an N^n array, with N the linear

grid size and n its dimensionality), is equivalently represented as a source probability distribution centered on the agent (a $(2N - 1)^n$ array). This transformation, illustrated in Fig. 25, is applied to the belief state before using it as an input to the neural network.

b. *Architecture* We use a feedforward neural network with fully connected layers: the input layer, followed by N_{hidden} hidden layers with rectifier linear units (ReLU) activations, and a (linear) output layer. The network size (number of neurons per layer and number of hidden layers) was chosen such that more neurons does not increase performance any further. Typically we used $N_{\text{hidden}} = 3$ in most cases, and with an increasing number of neurons per layer for increasing problem sizes. Note that with this type of architecture the number of weights (and the training time) does not scale well with the input size, which is why we are restricted to small problem sizes \mathcal{L} . For larger input sizes, a common approach is to use convolutional neural networks. The assessment of whether this alternative architecture is suitable for the source-tracking problem is left to future work.

c. *Initialization* Neural networks were trained from scratch (random initial weights). Repeated trials with different random initializations yielded identical performance, which shows the robustness of our training procedure. The reproducibility of our results is illustrated in Fig. 26.

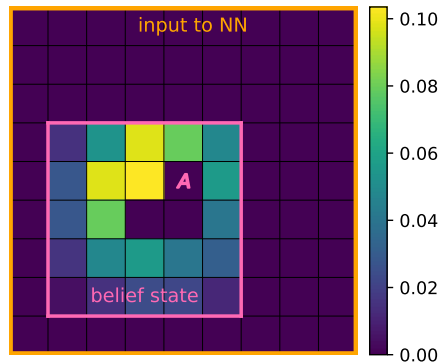


FIG. 25. Preprocessing: before being fed to the neural network, the belief state, which consists of the source probability distribution of size N^n (pink border) and of the agent’s position (depicted by a pink “A”), is transformed into a single probability distribution (orange border) of size $(2N - 1)^n$ centered on the agent.

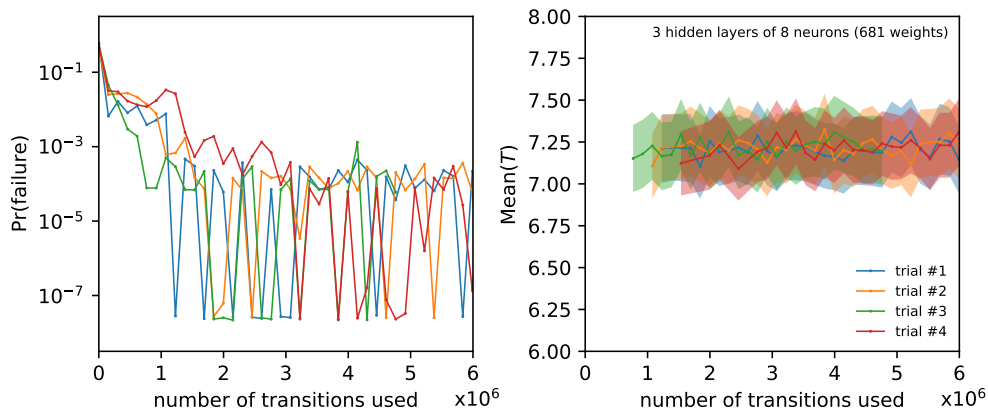


FIG. 26. Evolution of performance during training for a series of trials starting from different random initializations of the neural network weights (same case as in Fig. 21). Shaded areas show 95 % confidence intervals.

b. Training algorithm

The pseudo-code for our training algorithm is provided in Fig. 27. For the loss function, we used the mean square error, as defined in Eq. (56). We also experimented with the absolute relative error and did not find any significant difference. For exploration, we used ϵ -greedy with a value of ϵ that decays exponentially during the training. The hyperparameters we used are given in Table II. Note that these hyperparameters were not optimized (owing to the huge computational cost of such an optimization, which would have to be performed for each individual case), but chosen based on standard practice and preliminary trials. Training was performed on a single CPU with 8 cores, which leaves ample space for scaling up our approach to larger domains by parallelizing our algorithm (how to parallelize training is, however, not trivial).

Due to our choice of breaking ties arbitrarily in a deterministic manner (cf. Section II F 3), the symmetries of the agent trajectories are artificially broken (for example at the very beginning, where all actions are of equivalent value, the agent will always go left). This will

introduce a bias in the belief states sampled by agent (symmetric states will not be sampled equally often). In this context, an original feature of our algorithm is that we restore this symmetry during training by applying, at each agent step, a random symmetry transformation to the belief state. For example, in 1D, a belief state and its mirror image (flip along the axis) are equivalent, so the belief state is flipped with a probability of 1/2. Similarly, there are 8 equivalent belief states in 2D (symmetries of the square) and 48 in 3D (symmetries of the cube), amongst which we choose randomly at each agent step. Informal trials suggest that this trick allows to learn faster the relevant symmetries (that is, to assign equal values to symmetric belief states).

An alternative way would be to enforce symmetry constraints within the neural network. Informal trials indicate that this approach yield slower, less successful training. Similarly, enforcing concavity (a property that must be satisfied by the optimal value function) within the neural network seems to degrade training. We leave the detailed study of these interesting questions to future work.

hyperparameter	value	description
learning rate	0.001	for stochastic gradient descent (SGD)
discount factor	1.0	no discount
epsilon_init	1.0	initial value of ϵ in ϵ -greedy exploration
epsilon_floor	0.1	final value of ϵ in ϵ -greedy exploration
epsilon_decay	[1000,10000]	time scale for decay of ϵ , in number of training iterations
memory_size	[5000,100000]	minibatches are sampled from this number of transitions stored in memory
minibatch_size	64	number of transitions (s,a,s') over which each SGD update is computed
new_transitions_per_it	192	number of transitions added to memory at each training iteration
gd_steps_per_it	12	number of SGD updates performed at each training iteration
update_target_network_it	1	the target network is updated every this number of training iterations

TABLE II. List of hyperparameters (as usually defined or defined in our algorithm Fig. 27) and their values. When ranges are given, larger values are typically used for larger numbers of dimensions and problem sizes.

```

Initialize replay memory to capacity memory_size
Initialize value function  $v$  with random weights  $w$ 
Initialize target value function  $v^-$  with random weights  $w^- = w$ 
converged_weights  $\leftarrow$  False
it  $\leftarrow$  0
while not converged_weights do
    // Generate new experience
    epsilon  $\leftarrow$  max(epsilon_init * exp(-it/epsilon_decay), epsilon_floor) // decaying  $\epsilon$  for  $\epsilon$ -greedy exploration
    m  $\leftarrow$  0
    episode_complete  $\leftarrow$  True
    while m < new_transitions_per_it do
        if episode_complete then
            initialize belief state  $s$  for a new episode
            episode_complete  $\leftarrow$  False
        end if
        s  $\leftarrow$  apply_random_symmetry(s) // randomize over symmetries of the problem
        for all actions  $a$ , compute all  $s'$  accessible from  $s$  (i.e. all outcomes (found/not found and hits))
        store  $(s, a, s')$  in replay memory
        m  $\leftarrow$  m + 1
        with probability epsilon select a random action  $a$ ,
        otherwise select action  $a = \operatorname{argmin}_a \sum_{s'} \Pr(s'|s, a)[1 + v(s'; w)]$  // according to current policy
        s  $\leftarrow$  make_step_in_env(s, a) // transition to a new belief state according to action
        episode_complete  $\leftarrow$  is_episode_complete(s)
    end while
    // Update weights by stochastic gradient descent
    for gd_step = 1, gd_steps_per_it do
        Sample minibatch_size transitions  $(s, a, s')$  from replay memory
        For each transition, compute targets  $y = \min_a \sum_{s'} \Pr(s'|s, a)[1 + v^-(s'; w^-)]$  // RHS of Eq. (55) using
        delayed target network
        Perform a gradient descent step on  $(y - v(s; w))^2$  with respect to the network parameters  $w$ 
    end for

    converged_weights  $\leftarrow$  are_weights_converged()
    it  $\leftarrow$  it + 1
    every update_target_network_it iterations, reset  $v^- = v$ 
end while

```

FIG. 27. Pseudo-code for our training algorithm.

- [1] N. J. Vickers, Mechanisms of animal navigation in odor plumes, *The Biological Bulletin* **198**, 203 (2000).
- [2] B. S. Hansson, ed., *Insect Olfaction* (Springer, Berlin, 1999).
- [3] J. Murlis, J. S. Elkinton, and R. T. Carde, Odor Plumes and How Insects Use Them, *Annual review of entomology* **37**, 505 (1992).
- [4] T. Kiørboe, *A Mechanistic Approach to Plankton Ecology* (Princeton University Press, Princeton, 2008).
- [5] M. Vergassola, E. Villermaux, and B. I. Shraiman, "Infotaxis" as a strategy for searching without gradients, *Nature* **445**, 406 (2007).
- [6] A. Celani, E. Villermaux, and M. Vergassola, Odor Landscapes in Turbulent Environments, *Physical Review X* **4**, 041015 (2014).
- [7] S. D. Patek, On partially observed stochastic shortest path problems, in *Proceedings of the 40th IEEE Conference on Decision and Control*, Vol. 5 (2001) pp. 5050–5055.
- [8] S. D. Patek, Partially Observed Stochastic Shortest Path Problems With Approximate Solution by Neurodynamic Programming, *IEEE Transactions on Systems, Man, and Cybernetics - Part A: Systems and Humans* **37**, 710 (2007).
- [9] K. Chatterjee, M. Chmelik, R. Gupta, and A. Kanodia, Optimal cost almost-sure reachability in POMDPs, *Artificial Intelligence* **234**, 26 (2016).
- [10] G. Shani, J. Pineau, and R. Kaplow, A survey of point-based POMDP solvers, *Autonomous Agents and Multi-Agent Systems* **27**, 1 (2013).
- [11] M. J. Kochenderfer, T. A. Wheeler, and K. H. Wray, *Algorithms for Decision Making* (MIT Press, 2022).
- [12] H. Kurniawati, Partially Observable Markov Decision Processes (POMDPs) and Robotics, arXiv:2107.07599 [cs] (2021), arXiv:2107.07599 [cs].
- [13] M. Hauskrecht, Value-Function Approximations for Partially Observable Markov Decision Processes, *Journal of Artificial Intelligence Research* **13**, 33 (2000).
- [14] S. Ross, J. Pineau, S. Paquet, and B. Chaib-draa, Online Planning Algorithms for POMDPs, *Journal of Artificial Intelligence Research* **32**, 663 (2008).
- [15] R. S. Sutton and A. G. Barto, *Reinforcement Learning: An Introduction*, 2nd ed. (Bradford Books, 2018).
- [16] A. R. Cassandra, L. P. Kaelbling, and J. A. Kurien, Acting under uncertainty: Discrete Bayesian models for mobile-robot navigation, in *Proceedings of IEEE/RSJ International Conference on Intelligent Robots and Systems. IROS '96*, Vol. 2 (IEEE, 1996) pp. 963–972.
- [17] S. Thrun, W. Burgard, and D. Fox, *Probabilistic Robotics* (MIT Press, 2006).
- [18] E. M. Moraud and D. Martinez, Effectiveness and robustness of robot infotaxis for searching in dilute conditions, *Frontiers in Neurobotics* **4**, 1 (2010).
- [19] J.-B. Masson, Olfactory searches with limited space perception, *Proceedings of the National Academy of Sciences of the United States of America* **110**, 11261 (2013).
- [20] J.-B. Masson, M. Bailly Bechet, and M. Vergassola, Chasing information to search in random environments, *Journal of Physics A: Mathematical and Theoretical* **42**, 434009 (2009).
- [21] J. D. Rodriguez, D. Gomez-Ullate, and C. Mejia-Monasterio, Geometry-induced fluctuations of olfactory searches in bounded domains, *Physical Review E* **89**, 042145 (2014).
- [22] C. Barbieri, S. Cocco, and R. Monasson, On the trajectories and performance of Infotaxis, an information-based greedy search algorithm, *EPL (Europhysics Letters)* **94**, 20005 (2011).
- [23] E. D. Karpas, A. Shklarsh, and E. Schneidman, Information socialtaxis and efficient collective behavior emerging in groups of information-seeking agents, *Proceedings of the National Academy of Sciences* **114**, 5589 (2017).
- [24] M. Hutchinson, H. Oh, and W.-H. Chen, Entrotaxis as a strategy for autonomous search and source reconstruction in turbulent conditions, *Information Fusion* **42**, 179 (2018).
- [25] C. Chen, T. D. Murphey, and M. A. MacIver, Tuning movement for sensing in an uncertain world, *eLife* **9**, e52371 (2020), 32959777.
- [26] N. Voges, A. Chaffiol, P. Lucas, and D. Martinez, Reactive Searching and Infotaxis in Odor Source Localization, *PLOS Computational Biology* **10**, e1003861 (2014).
- [27] A. J. Calhoun, S. H. Chalasani, and T. O. Sharpee, Maximally informative foraging by *Caenorhabditis elegans*, *eLife* **3**, 10.7554/eLife.04220 (2014).
- [28] B. Ristic, A. Skvortsov, and A. Gunatilaka, A study of cognitive strategies for an autonomous search, *Information Fusion* **28**, 1 (2016).
- [29] A. W. Eggels, R. P. J. Kunnen, B. Koren, and A. S. Tijsseling, Infotaxis in a turbulent 3D channel flow, *Journal of Computational and Applied Mathematics* **310**, 44 (2017).
- [30] J. D. Rodriguez, D. Gomez-Ullate, and C. Mejia-Monasterio, On the performance of blind-infotaxis under inaccurate modeling of the environment, *The European Physical Journal Special Topics* **226**, 2407 (2017).
- [31] R. E. Bellman, *Dynamic Programming* (Princeton University Press, 1957).
- [32] R. A. Baeza-Yates, J. C. Culberson, and G. J. E. Rawlins, Searching in the Plane, *Information and Computation* **106**, 234 (1993).
- [33] D. J. C. MacKay, *Information Theory, Inference and Learning Algorithms* (Cambridge University Press, Cambridge, 2005).
- [34] E. J. Sondik, *The Optimal Control of Partially Observable Markov Decision Processes*, Ph.D. thesis, Stanford University (1971).
- [35] R. D. Smallwood and E. J. Sondik, The Optimal Control of Partially Observable Markov Processes over a Finite Horizon, *Operations Research* **21**, 1071 (1973).
- [36] V. Mnih, K. Kavukcuoglu, D. Silver, A. A. Rusu, J. Veness, M. G. Bellemare, A. Graves, M. Riedmiller, A. K. Fidjeland, G. Ostrovski, S. Petersen, C. Beattie, A. Sadik, I. Antonoglou, H. King, D. Kumaran, D. Wierstra, S. Legg, and D. Hassabis, Human-level control through deep reinforcement learning, *Nature* **518**, 529 (2015).
- [37] L. P. Kaelbling, M. L. Littman, and A. R. Cassandra, Planning and acting in partially observable stochastic domains, *Artificial Intelligence* **101**, 99 (1998).
- [38] R. T. Cardé, Navigation Along Windborne Plumes of Pheromone and Resource-Linked Odors, *Annual Review*

- of *Entomology* **66**, 317 (2021).
- [39] B. Hartl, M. Hübl, G. Kahl, and A. Zöttl, Microswimmers learning chemotaxis with genetic algorithms, *Proceedings of the National Academy of Sciences* **118**, 10.1073/pnas.2019683118 (2021).
- [40] G. Reddy, A. Celani, T. J. Sejnowski, and M. Vergassola, Learning to soar in turbulent environments, *Proceedings of the National Academy of Sciences of the United States of America* **113**, E4877 (2016).
- [41] G. Reddy, J. Wong-Ng, A. Celani, T. J. Sejnowski, and M. Vergassola, Glider soaring via reinforcement learning in the field, *Nature* **562**, 236 (2018).
- [42] S. Colabrese, K. Gustavsson, A. Celani, and L. Biferale, Flow Navigation by Smart Microswimmers via Reinforcement Learning, *Physical Review Letters* **118**, 158004 (2017).
- [43] K. Gustavsson, L. Biferale, A. Celani, and S. Colabrese, Finding efficient swimming strategies in a three-dimensional chaotic flow by reinforcement learning, *The European Physical Journal E* **40**, 110 (2017).
- [44] J. K. Alageshan, A. K. Verma, J. Bec, and R. Pandit, Machine learning strategies for path-planning microswimmers in turbulent flows, *Physical Review E* **101**, 043110 (2020).
- [45] R. Monthiller, A. Loisy, M. A. R. Koehl, B. Favier, and C. Eloy, Surfing on turbulence, arXiv:2110.10409 [physics] (2021), arXiv:2110.10409 [physics].
- [46] R. M. Macnab and D. E. Koshland, The Gradient-Sensing Mechanism in Bacterial Chemotaxis, *Proceedings of the National Academy of Sciences* **69**, 2509 (1972).
- [47] G. Lan and Y. Tu, Information processing in bacteria: Memory, computation, and statistical physics: A key issues review, *Reports on Progress in Physics* **79**, 052601 (2016).
- [48] M. v. Smoluchowski, Versuch einer mathematischen theorie der koagulationskinetic kolloider Lösungen, *Zeitschrift für Physikalische Chemie* **92**, 129 (1917).
- [49] H. C. Berg and E. M. Purcell, Physics of chemoreception, *Biophysical journal* **20**, 193 (1977).